APPENDIX A: SUMMARY OF RADIATION EXCHANGE FACTORS FOUND IN LITERATURE

This appendix summarises all the radiation exchange factors and relevant data found in literature.

Table A.1: Summary of radiation exchange factors

RESEARCHER/S	RADIATION EXCHANGE FACTOR F_E	COMMENTS
Chen & Churchill (1963:35)	$F_E = \frac{2}{d_p(a+2b)}$	Need absorption and scattering coefficients for each packing
Waoka & Wato (1968:24)	$F_E = \frac{2}{(2/\varepsilon_r - 0.264)}$	—
Argo & Smith (1957:443)	$F_E = \frac{1}{(2/\varepsilon_r - 1)}$	—
Kasparek & Vortmeyer (1976:117)	$F_E = \frac{\varepsilon_r + B}{1-B}$	Has an empirical parameter $B = f(\varepsilon, \varepsilon_r)$. No general function is available to calculate B for different packings.
Vortmeyer (1978:532)	$F_E = \frac{2B + \varepsilon_r(1-B)}{2(1-B) - \varepsilon_r(1-B)}$	Has an empirical parameter $B = f(\varepsilon, \varepsilon_r)$. No general function is available to calculate B for different packings.
RESEARCHER/S	**RADIATION EXCHANGE FACTOR F_E^***	**COMMENTS**
Breitbach (1978:1)	$F_E^* = \left[\frac{\pi}{6}\frac{\psi}{1-\varepsilon}\cdot\left(1-\frac{\tau h(\Lambda_f,\varepsilon_r,\varepsilon)(1+\psi)}{1+\psi\tau h(\Lambda_f,\varepsilon_r,\varepsilon)}\right)\right]$ *for* $\varepsilon = 0.4$ *and* 0.48	Has an empirical parameter $B = f(\varepsilon, \varepsilon_r)$. No general function is available to calculate B for different packings. Only applicable for a porosity of $0.2 \le \varepsilon \le 0.476$.
Breitbach & Barthels (1980:392)	$F_E^* = \left\{\left[1-\sqrt{(1-\varepsilon)}\right]\varepsilon + \frac{\sqrt{(1-\varepsilon)}}{\frac{2}{\varepsilon_r}-1}\cdot\frac{B+1}{B}\cdot\frac{1}{1+\frac{1}{\left(\frac{2}{\varepsilon_r}-1\right)\Lambda_f}}\right\}$	Model more sensitive to porosity variations
Robold (1982:129)	$F_E^* = F_E\left[1-\chi\frac{\Delta_0}{1+\frac{k_s}{F_{E,0}4d_s^{\varepsilon}\sigma T^3}}\right]$ *for* $\varepsilon = 0.43$ & 0.395	Has an empirical parameter $B = f(\varepsilon, \varepsilon_r)$. No general function is available to calculate B for different packings. Only applicable for a porosity of $0.2 \le \varepsilon \le 0.476$.
Singh & Kaviany (1994:2579)	$F_E^* = a_1\varepsilon_r \tan^{-1}\left(a_2\frac{(\Lambda_f)^{a_3}}{\varepsilon_r}\right) + a_4$ *for* $\varepsilon = 0.476$	Only valid for $\varepsilon = 0.476$. Constants where obtained using a Monte Carlo method

		EMISSIVITY				
		0.20	*0.35*	*0.60*	*0.85*	*1.0*
RESEARCHER/S	**CALCULATION METHOD**	**RADIATION EXCHANGE VALUES F_E**				
Singh & Kaviany (1991:2869)	Monte Carlo (diffuse)	0.32	0.45	0.68	0.94	1.10
Singh & Kaviany (1991:2869)	Two-flux (diffuse)	0.88	0.91	1.02	1.06	1.11
Kasparek & Vortmeyer (1976:117)	Experimental measurements $(\varepsilon = 0.4)$	–	0.54	–	1.02	–

APPENDIX B: SUMMARY OF CORRELATIONS FOUND IN LITERATURE

Table B.1: Summary of correlations found in literature

RESEARCHER/S	DESCRIPTION	EQUATION	SECONDARY PARAMETERS				COMMENTS
			PRESSURE	RADIATION	CONTACT AREA OR ROUGHNESS	MACRO OR MICRO	
SOLID AND FLUID EFFECTIVE THERMAL CONDUCTIVITY							
Diessler & Boegli (1958)	One-dimensional, series and parallel layers	(3.6) (3.8)	N	N	None	Macro	Two models act as bounds for effective thermal conductivity at low temperatures
Kunii & Smith (1960)	One-dimensional, semi-empirical, lumped parameter	(3.9)	N	N	None	Macro	Highly empirical model
Zehner & Schlünder (1970:933)	Two-dimensional, semi-empirical	(3.20)	N	N	None	Macro	Uses a cylindrical unit cell to do effective thermal conductivity calculations
Okazaki *et al.* (1977:164)	One-dimensional, structured based, semi-empirical	(3.26)	N	N	None	Macro	Model over-predicts effective thermal conductivity
Batchelor & O'Brien (1977:313)	One-dimensional, empirical	(3.28)	N	N	None	Macro	Highly empirical and valid for the bulk region of a packed bed
Hsu *et al.* (1995:265) (Square Cylinder Model)	Two-dimensional, semi-empirical, lumped parameter	(3.33)	N	N	Contact area calculated empirically	Macro	Obtain empirical constants by comparing model to various experimental measurements of different pebble diameters and porosities
Hsu *et al.* (1995:266) (Circular Cylinder Model)	Two-dimensional, semi-empirical	(3.41) (3.42) (3.43)	N	N	Contact area calculated empirically	Macro	Obtain empirical constants by comparing model to various experimental measurements of different pebble diameters and porosities
Hsu *et al.* (1995:267) (Cube Model)	Three-dimensional, semi-empirical	(3.44)	N	N	Contact area calculated empirically	Macro	Obtain empirical constants by comparing model to various experimental measurements of different pebble diameters and porosities
Cheng *et al.* (1999:4199)	Three-dimensional, structured based	Model A (3.51) (3.54) Model B (3.62) (3.55)	N	N	Contact area	Micro	Need coordinates of a numerical packed bed and Voronoi polyhedra volumes to do calculations

RESEARCHER/S	DESCRIPTION	EQUATION	SECONDARY PARAMETERS				COMMENTS
			PRESSURE	RADIATION	CONTACT AREA OR ROUGHNESS	MACRO OR MICRO	
Siu & Lee (2000:3917)	Three-dimensional, semi-empirical, structured based	(3.67)	N	N	Contact area	Micro	Does not account for fluid phase; assign a certain structure to a specific porosity range; use a resistance model.
Slavin *et al.* (2002:4151)	Two-dimensional, semi-empirical	(3.76) (3.77)	Y	Y	Contact area and roughness	Semi -micro	Model was developed for small spheres. Therefore, much attention was given to the Knudsen regime. A view factor of one is assumed for radiative heat transfer.
Shapiro *et al.* (2004:268)	Two-dimensional empirical	(3.86)	Y	N	Contact area calculated empirically	Macro	Model was developed for very small spheres. Use an empirical constant to fit model to experimental data.
CONTACT AREA OR ROUGHNESS EFFECTIVE THERMAL CONDUCTIVITY							
Bauer & Schlünder (1978:189)	Two-dimensional, semi-empirical	(3.89)	Y	Y	Contact area calculated empirically	Macro	Model applicable only in the bulk porosity region of a packed bed
Hsu *et al.* (1994:2751)	Two-dimensional semi-empirical	(3.99)	N	N	Contact area	Macro	Use Zehner & Schlünder (1970:933) model with different integration parameters.
Kaviany (1991:127)	Two-dimensional	(3.102)	N	N	Contact area	Macro	Model only applicable for certain porosity ranges
Bahrami *et al.* (2006:3691)	Three-dimensional, semi-empirical, structured based	(3.104)	Y	N	Contact area and roughness	Micro	Very detailed model accounting for various conditions
RADIATION EFFECTIVE THERMAL CONDUCTIVITY							
Kunii & Smith (1960:71) Yagi & Kunii (1957:373)	One dimensional, semi-empirical, lumped parameter	(3.130)	N	Y	None	Macro	Same model as Model 2 in Section 3.1.2, only radiation added; analysis has shown that the correlation is incorrect at higher porosities.
Chen & Churchill (1963:35)	Two dimensional, empirical	(3.134)	N	Y	None	Macro	Model based on experimental results; not applicable in general
Vortmeyer (1982:2751)	Two-dimensional, semi-empirical	(3.144)	N	Y	None	Macro	Model highly dependent on empirical radiation transmission parameter
Breitbach & Barthels (1980:392)	Two-dimensional, semi-empirical	(3.150)	N	Y	None	Macro	Modified the original Zehner & Schlünder (1970:933) radiation equation
Robold (1982:1)	Two-dimensional, semi-empirical	(3.162)	N	Y	Contact area	Macro	Model highly dependent on empirical radiation transmission parameter; only valid for a porosity up to 0.43
Singh & Kaviany (1994:2579)	Two-dimensional, empirical	(3.166)	N	Y	None	Macro	Empirical constants obtained from a curve fit (Monte Carlo analysis for a SC packing)

RESEARCHER/S	DESCRIPTION	EQUATION	SECONDARY PARAMETERS				COMMENTS
			PRESSURE	RADIATION	CONTACT AREA OR ROUGHNESS	MACRO OR MICRO	
Cheng *et al.* (2002:1)	Two-dimensional, structure based model	(3.167)	N	Y	None	Micro	Model is used in conjunction with model proposed by Cheng *et al.* (1999:4199)
WALL EFFECTIVE THERMAL CONDUCTIVITY							
Yagi & Kunii (1961:760)	One-dimensional, semi-empirical, lumped parameter	(3.168)	N	Y	None	Macro	Discontinuity at the start of the near-wall region; radiation prediction is incorrect
Robold (1982:1)	Two-dimensional, semi-empirical	(3.182)	N	Y	None	Macro	Only applicable for $d_p = 1/2$ away from the wall; correlation is highly empirical
Tsotsas (2002)	Two-dimensional, semi-empirical	(3.183)	Y	Y	None	Macro	Discontinuities arise for effective thermal conductivity at wall

APPENDIX C: EXPERIMENTAL TEST FACILITIES FOUND IN LITERATURE

This appendix provides a brief overview of other experimental test facilities used to obtain experimental data to assist in the validation of the Multi-sphere Unit Cell Model.

C.1 SPHERICAL-FLAT CONTACT EXPERIMENTAL TEST FACILITY

Kitscha & Yovanovich (1974:93) conducted experiments to obtain the overall thermal resistances between a steel sphere and a flat surface as presented in Figure C.1. The load was varied to study the effect it has on the overall solid and gas conduction. For each constant load, the gas pressure was varied from vacuum to atmospheric conditions. Tests were conducted using two different gases: air and argon. However, for this study only argon was considered. The test section was well insulated and tests were conducted in a 70°C to 90°C temperature range. Material properties and experimental and simulation results considered in this study are presented in Table C.1 and Table C.2.

Table C.1: Physical and thermal properties of test specimens

SPECIMEN	POISSON'S RATIO	MODULUS OF ELASTICITY	THERMAL CONDUCTIVITY	SURFACE ROUGHNESS
Flat (1020 carbon steel)	0.3	4.35 GPa	17.63 W/mK	0.13 μm
Sphere (1020 carbon steel) $d_p = 25.4mm$	0.3	4.35 GPa	16.76 W/mK	–

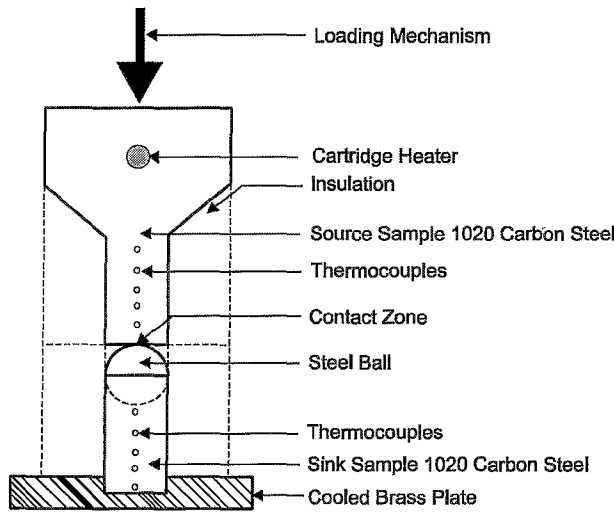

Figure C.1: Sphere-flat contact experimental setup (Kitscha & Yovanovich, 1974:93)

Table C.2: Experimental results for argon tests

GAS	APPLIED FORCE [N]	GAS PRESSURE [kPa]	THERMAL RESISTANCE [K/W]	UNCERTAINTY 4.65%	SIMULATION RESULTS	% DIFF.
Argon	16	0.0733	51.60	2.4	67.70	23.79
		0.1	52.35	2.43	66.22	20.94
		0.147	52.92	2.46	64.49	17.94
		0.267	52.73	2.45	62.03	14.99
		0.28	50.65	2.36	61.85	18.11
		0.613	50.27	2.34	59.00	14.80
		0.653	51.98	2.42	58.78	11.58
		1.333	47.99	2.23	56.50	15.06
		10.667	44.96	2.09	50.79	11.49
		13.333	44.39	2.06	50.22	11.61
		26.667	42.87	1.99	48.51	11.63
		53.333	44.58	2.07	46.86	4.87
		80	42.30	1.97	45.94	7.92
		98.667	44.20	2.06	45.48	2.82
	55.6	0.00667	57.10	2.65	54.57	4.63
		0.024	50.08	2.33	47.67	5.05
		0.0933	45.53	2.12	45.24	0.63
		0.32	43.82	2.04	43.39	0.99
		2.667	39.65	1.84	40.62	2.40
		13.333	37.56	1.75	38.51	2.47
		53.333	37.18	1.73	36.65	1.44
		98.667	36.99	1.72	35.86	3.15
	195.7	0.02	34.52	1.61	31.63	9.15
		0.0533	33.20	1.54	31.28	6.12
		0.16	32.63	1.52	30.95	5.42
		2.667	30.16	1.40	29.92	0.80
		13.333	30.16	1.40	28.91	4.33
		53.333	29.97	1.39	27.95	7.23
		98.667	29.97	1.39	27.56	8.75
	467	0.08	24.85	1.16	24.12	3.02
		0.4	23.90	1.11	24.31	1.68
		2.667	23.14	1.08	24.08	3.89
		14.667	22.76	1.06	23.45	2.93
		60	22.95	1.07	22.89	0.27
		98.667	22.76	1.06	22.72	0.19

Bahrami *et al.* (2006:3696) stated that the effective microhardness is $H_{mic} = 4\,GPa$. Additional gas parameters were also given by Bahrami *et al.* (2006:3696), as presented in Table C.3.

Table C.3: Gas parameters (Bahrami et al., 2006:3696)

GAS	PRANDTL NUMBER	SPECIFIC GAS RATIO $\gamma_g = c_p/c_v$	ACCOMMODATION COEFFICIENT	MEAN FREE PATH AT REFERENCE PRESSURE	THERMAL CONDUCTIVITY OF GAS
Argon	0.67	1.67	0.90	66.66 nm	$k_{argon}(W/mK) = 0.0159 + 4x10^{-6}T(K)$

C.2 SPHERICAL-SPHERICAL CONTACT EXPERIMENTAL TEST FACILITY

Buonanno *et al.* (2003:251) conducted experiments to determine the effective thermal conductivity through 100Cr6 steel and AlMgSi 6060 aluminium alloy spheres. Tests were conducted using SC- and FCC-packed structures, with air as the interstitial gas at atmospheric conditions. The effective thermal conductivity results were obtained by varying the surface roughness of the packings, as well as the average applied force with a specific surface roughness configuration. In this study, only the experimental results of the 100Cr6 steel were considered. Bahrami *et al.* (2006:3696) gave a simplistic description of the experimental apparatus displayed in Figure C.2.

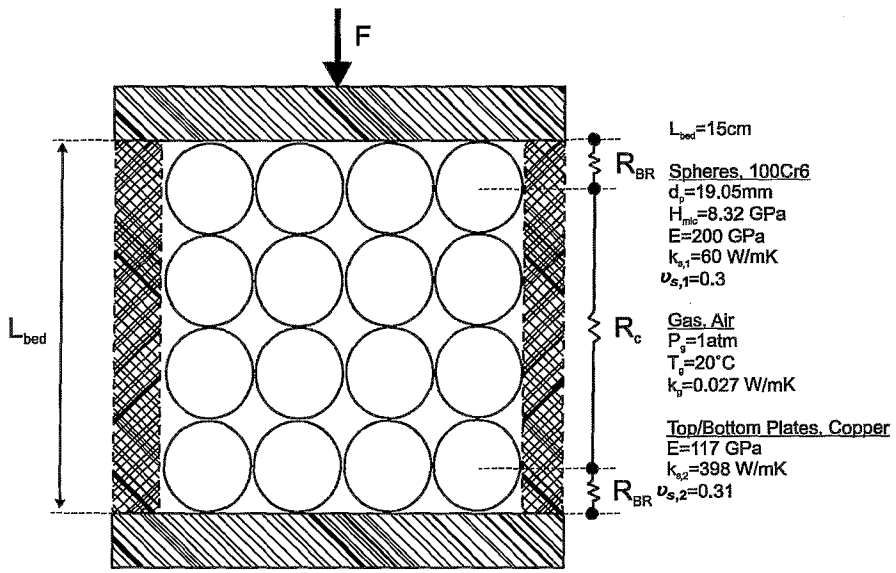

Figure C.2: Buonanno et al. experimental apparatus for a Simple Cubic packing (Buonanno et al., 2003:251)

Heat enters the packed bed at the top copper plate and leaves the packing at the bottom copper plate. The sides of the packing were well insulated, ensuring a one-dimensional heat transfer. It should be noted, however, that Buonanno *et al.* (2003:251) measured the total effective thermal conductivity of the bed, which included the boundary thermal resistances at

the top and bottom copper plates. The experimental and the simulation results are displayed in Table C.4.

Table C.4: Experimental and simulation results for Buonanno et al. experimental tests (Buonanno et al., 2003:251)

GAS	PACKING ARRANGEMENT	APPLIED FORCE [N]	SURFACE ROUGHNESS [μm]	TOTAL EFFECTIVE THERMAL CONDUCTIVITY [W/mK]	UNCERTAINTY	SIMULATION RESULTS	% DIFF.
Air	SC	0.983	0.03	0.465	0.0321	0.4558	2.02
			0.16	0.455	0.0314	0.4357	4.43
			0.97	0.395	0.0273	0.4017	1.67
			1.36	0.39	0.0269	0.3935	0.09
			1.7	0.365	0.0252	0.3875	5.81
Air	SC	0.983	0.03	0.464	0.036	0.4558	1.80
		1.96		0.480	0.0267	0.4866	1.36
		2.95		0.505	0.0279	0.5132	1.60
		3.93		0.510	0.0281	0.5365	4.94
Air	FCC	0.783	0.03	0.680	0.0275	0.6014	13.07
			0.16	0.670	0.0275	0.5781	15.90
			0.97	0.590	0.0260	0.5368	9.91
			1.36	0.550	0.0260	0.5266	4.44
			1.7	0.525	0.0260	0.519	1.16
Air	FCC	0.793	0.03	0.679	0.0387	0.6019	12.81
		1.49		0.703	0.0363	0.6334	10.99
		2.18		0.706	0.0361	0.6607	6.86
		2.87		0.718	0.0364	0.6854	4.76

C.3 HIGH TEMPERATURE OVEN EXPERIMENTAL TEST FACILITY

Robold (1982:156) and Breitbach & Barthels (1980:396) conducted various experimental tests on the HTO experimental test facility. The test facility consisted of a cylindrical graphite vessel containing the randomly packed bed with a diameter of 0.5 m and a height of 0.7 m. Heat was inserted by an induction-heating coil, situated outside the cylindrical packed bed. Tests were conducted at two different pressures, which were vacuum and between 70 to 85 kPa, with helium as the interstitial gas. A radial symmetrical temperature profile was obtained by limiting the heat loss in the axial direction through the placing of insulation at the top and bottom surfaces. The test facility is displayed in Figure C.3 and a test summary is displayed in Table C.5. It is important to note that effective thermal conductivity values were extracted in the bulk region and wall region between the sphere and graphite reflector.

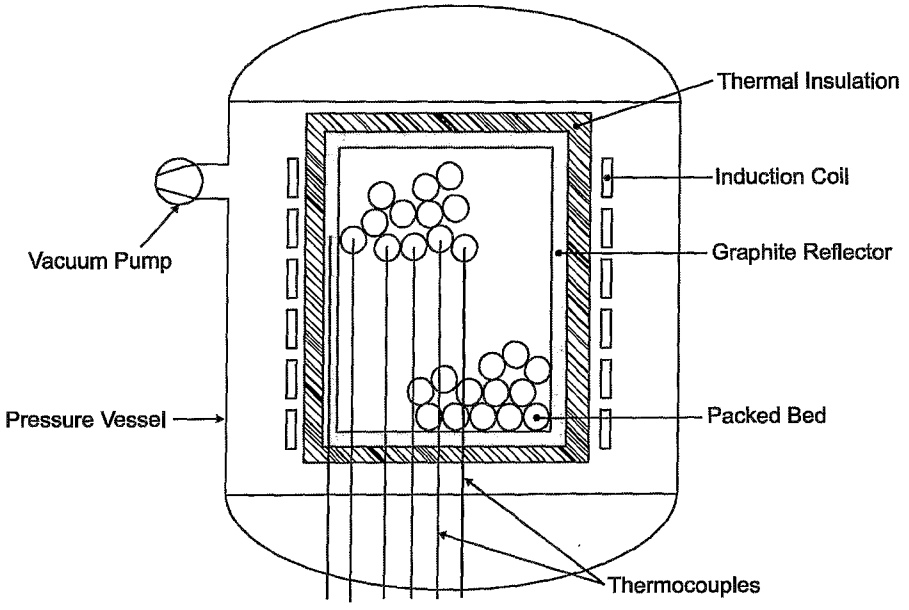

Figure C.3: High Temperature Oven
(Breitbach & Barthels, 1980:396)

Table C.5: Test summary
(Robold, 1982:109)

PEBBLE MATERIAL	PEBBLE DIAMETER	EXTRACTION REGION, k_{eff}	TEMPERATURE EXPERIMENTAL RANGE [K]	
			VACUUM	HELIUM
Graphite	$d_p = 40mm$	Bulk	$T = 400....1900$	
		Bulk		$T = 400....1200$
		Wall	$T = 600....1000$	
		Wall		$T = 600....1000$
Zirconium oxide (ZrO_2)	$d_p = 31.6mm$	Bulk	$T = 300....1700$	
		Bulk		$T = 300....1700$
		Wall	$T = 500....1300$	
		Wall		$T = 500....1300$
Steel	$d_p = 19mm$	Bulk	$T = 400....600$	
		Wall	$T = 400....600$	

It should be noted that Breitbach & Barthels (1980:395) also conducted experimental tests with ZrO_2 spheres of $d_p = 45mm$ and with graphite sphere of $d_p = 40mm$. However, in this study the experimental tests conducted with graphite sphere is considered and the relevant data is tabulated.

Table C.6: Material property summary (Robold, 1982:110)

TEMPERATURE [K]	300	500	700	900	1100	1300	1500	1700	1900
$k_{g,He}$ [W/mK]	0.16	0.22	0.28	0.34	0.39	0.44	0.48	0.52	0.56
$k_{s,Graphite}$ [W/mK]	52.0	40.5	33.7	29.2	26.0	23.3	21.2	19.2	17.3
$\varepsilon_{r,Graphite}$	0.7	0.78	0.85	0.88	0.88	0.9	0.89	0.89	0.88

A transient method described by Robold (1982:103) and Breitbach & Barthels (1980:395) was used to extract the effective thermal conductivity values. The results of the experimental tests are tabulated in Table C.7 to Table C.9.

Table C.7: Experimental test and simulation results for bulk region, $\bar{\varepsilon} = 0.39$, graphite spheres conducted in the High Temperature Oven (Robold, 1982:103)

VACUUM					HELIUM				
TEMP [K]	$k^r_{e,exp}$ [W/mK]	Unc	$k^r_{e,sim}$ [W/mK]	% DIFF	TEMP [K]	$k_{eff,exp}$ [W/mK]	Unc	$k_{eff,sim}$ [W/mK]	% DIFF.
410	0.2	0.01	0.45	55.62	417	1.18	0.03	3.46	65.86
445	0.21	0.01	0.58	63.56	450	1.2	0.03	3.64	67.01
475	0.45	0.01	0.70	35.76	467	1.45	0.04	3.74	61.18
512	0.6	0.02	0.88	31.51	482	1.5	0.04	3.83	60.78
540	0.8	0.02	1.03	22.03	501	1.66	0.04	3.94	57.89
584	1.03	0.03	1.29	20.34	522	1.92	0.05	4.08	52.9
630	1.25	0.03	1.62	22.65	550	1.94	0.05	4.27	54.55
668	1.4	0.04	1.92	26.97	570	2.1	0.05	4.41	52.40
685	2	0.05	2.06	3.05	590	2.28	0.06	4.56	50.01
720	2.15	0.05	2.38	9.74	613	2.45	0.06	4.74	48.33
764	2.56	0.06	2.82	9.35	636	2.80	0.07	4.93	43.23
784	2.75	0.07	3.04	9.54	665	3.00	0.08	5.18	42.13
822	3.40	0.09	3.48	2.21	695	3.30	0.08	5.46	39.59
847	3.85	0.10	3.78	1.77	722	3.30	0.08	5.73	42.40
884	3.85	0.10	4.26	9.71	741	3.85	0.10	5.93	35.02
918	4.65	0.12	4.74	1.80	769	4.10	0.10	6.23	34.16
942	4.98	0.12	5.09	2.06	820	4.65	0.12	6.82	31.83
965	5.25	0.13	5.43	3.37	868	5.28	0.13	7.43	28.97
1003	6.00	0.15	6.04	0.61	922	5.97	0.15	8.18	27.05
1038	6.25	0.16	6.62	5.65	971	6.68	0.17	8.93	25.15
1067	6.60	0.17	7.13	7.47	1021	7.40	0.19	9.74	24.02
1104	7.35	0.18	7.81	5.93	1060	7.72	0.19	10.42	25.91
1141	7.52	0.19	8.53	11.80	1086	8.28	0.21	10.89	23.97
1160	8.05	0.20	8.91	9.61	1122	9.00	0.23	11.57	22.21
1198	8.80	0.22	9.69	9.18	1165	9.70	0.24	12.42	21.90
1235	9.05	0.23	10.49	13.73	1213	10.38	0.26	13.42	22.65
1257	9.76	0.24	10.98	11.11	1266	11.18	0.28	14.60	23.42
1285	10.59	0.26	11.62	8.86	1310	11.85	0.30	15.62	24.14
1328	11.25	0.28	12.64	11.00	1345	12.65	0.32	16.47	23.19
1383	12.11	0.30	14.02	13.62	1382	13.17	0.33	17.40	24.31

VACUUM					HELIUM				
TEMP [K]	$k^r_{e,exp}$ [W/mK]	Unc	$k^r_{e,sim}$ [W/mK]	% DIFF	TEMP [K]	$k_{eff,exp}$ [W/mK]	Unc	$k_{eff,sim}$ [W/mK]	% DIFF.
1432	13.14	0.33	15.30	14.12	1413	13.58	0.34	18.21	25.43
1462	13.50	0.34	16.12	16.25	1453	14.22	0.36	19.28	26.24
1493	14.05	0.35	16.99	17.30	1497	14.90	0.37	20.49	27.28
1528	14.65	0.37	17.99	18.57	1542	15.60	0.39	21.78	28.37
1567	15.32	0.38	19.14	19.96	1578	16.10	0.40	22.85	29.54
1619	15.80	0.28	20.73	23.78	1623	16.76	0.30	24.21	30.77
1658	16.35	0.29	21.96	25.55	1660	17.20	0.31	25.37	32.20
1700	17.18	0.31	23.32	26.33	1683	17.50	0.32	26.09	32.92
1765	17.85	0.32	25.49	29.97	1700	18.00	0.32	26.64	32.43
1797	18.50	0.33	26.59	30.42	1728	18.05	0.33	27.54	34.46
1837	18.85	0.34	27.98	32.63	1752	18.52	0.34	28.33	34.63
1875	19.45	0.35	29.32	33.66	1795	19.00	0.35	29.75	36.13
					1835	19.45	0.36	31.10	37.46
					1891	20.05	0.36	33.00	39.24

Table C.8: Experimental test results for bulk region, $\bar{\varepsilon} = 0.39$, graphite spheres conducted in the High Temperature Oven (Breitbach & Barthels, 1980:395)

VACUUM			
TEMP [K]	$k^r_{e,exp}$ [W/mK]	TEMP [K]	$k^r_{e,exp}$ [W/mK]
718.15	2	1355.15	13.4
748.15	2.5	1363.15	11.9
823.15	3.2	1429.15	13.4
873.15	3.5	1448.15	12.95
923.15	5	1450.15	15.7
973.15	5.1	1470.15	14.3
1003.15	5.8	1493.15	14.5
1053.15	6	1553.15	17.4
1088.15	8.1	1583.15	16
1098.15	7.5	1585.15	17.5
1118.15	7.15	1648.15	17.8
1138.15	8.5	1698.15	19.8
1198.15	9.7	1768.15	21.5
1223.15	10.9	1784.15	18.6
1268.15	11.25	1818.15	21.7
1284.15	10.92	1835.15	19.3
1307.15	11.5	1841.15	22.2
1331.15	13.2	1863.15	19.55

Table C.9: Experimental test and simulation results for wall region, graphite spheres conducted in the High Temperature Oven (Robold, 1982:103)

VACUUM					HELIUM				
TEMP [K]	$k^r_{e,exp}$ [W/mK]	Unc	$k^r_{e,sim}$ [W/mK]	% DIFF	TEMP [K]	$k_{eff,exp}$ [W/mK]	Unc	$k_{eff,sim}$ [W/mK]	% DIFF.
611	0.91	0.27	1.11	18.09	611	1.78	0.27	3.26	45.31
669	1.3	0.27	1.45	10.59	667	2.18	0.27	3.62	39.85
720	1.66	0.27	1.81	8.03	720	2.61	0.27	4.02	35.03
773	2.1	0.27	2.22	5.32	774	3.07	0.27	4.46	31.23
835	2.64	0.27	2.77	4.59	837	3.62	0.27	5.05	28.27
896	3.17	0.27	3.38	6.16	897	4.2	0.27	5.67	25.89
					993	5.34	0.27	6.79	21.38

C.4 SANA-I EXPERIMENTAL TEST FACILITY

This section provides a brief overview of the SANA-I experimental facility. Material and gas properties are shown in Figure C.6 and Figure C.7.

The test facility investigated the heat transfer mechanisms inside the core of a High Temperature Gas-cooled Reactor (HTGR). The SANA-I experimental test facility had a central heater element with a diameter of 0.13 m and an outer cylindrical diameter of 1.5 m. Two different sized graphite pebble diameters were used namely $d_p = 60mm$ and $d_p = 30mm$, in a randomly packed arrangement with a bed height of $L_{bed} = 1m$. Temperature measurements are tabulated in Table C.10 and Table C.11, where extracted effective thermal conductivity is shown in Table C.12 to Table C. 14. Tests were conducted at $P_g = 1atm$.

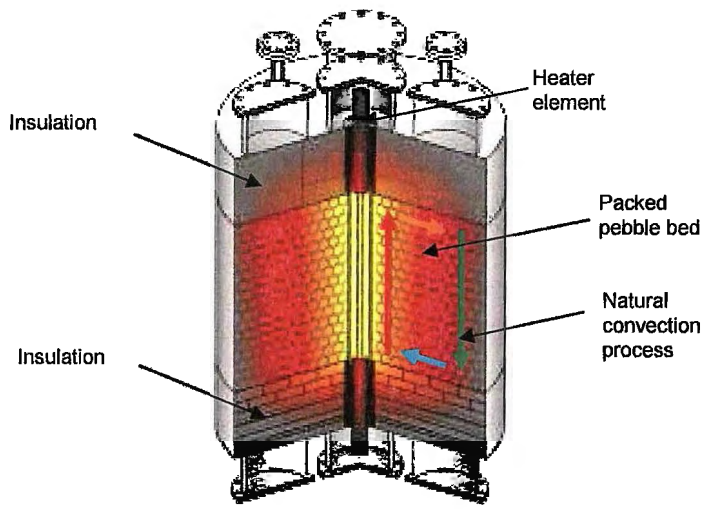

Figure C.4: SANA-I experimental test facility (Stöcker, 1998:44)

Table C.10: Temperature measurements of the SANA-I experimental test facility (10kW long heater) (Stöcker, 1998:44)

			RADIUS [m]							
INPUT POWER [kW]			0.065	0.1	0.22	0.34	0.46	0.58	0.70	0.756
P_{Brutto}	10.00 kW	HEIGHT [m]				Temp [°C]				
$P_{Heating\ element}$	8.91 kW	0.91	565	488	372	311	256	203	168	124
$P_{Electrode}$	0.62 kW	0.5	552	450	337	284	233	187	157	130
P_{Loss}	0.47 kW	0.09	491	389	301	240	201	166	132	105

Table C.11: Temperature measurements of the SANA-I experimental test facility (35kW long heater) (Stöcker, 1998:44)

			RADIUS [m]							
INPUT POWER [kW]			0.065	0.1	0.22	0.34	0.46	0.58	0.70	0.756
P_{Brutto}	35.02 kW	HEIGHT [m]				Temp [°C]				
$P_{Heating\ element}$	32.02 kW	0.91	1151	1016	827	715	603	485	398	279
$P_{Electrode}$	1.94 kW	0.5	1148	987	806	704	600	486	393	303
P_{Loss}	1.06 kW	0.09	1119	948	788	658	580	461	356	264

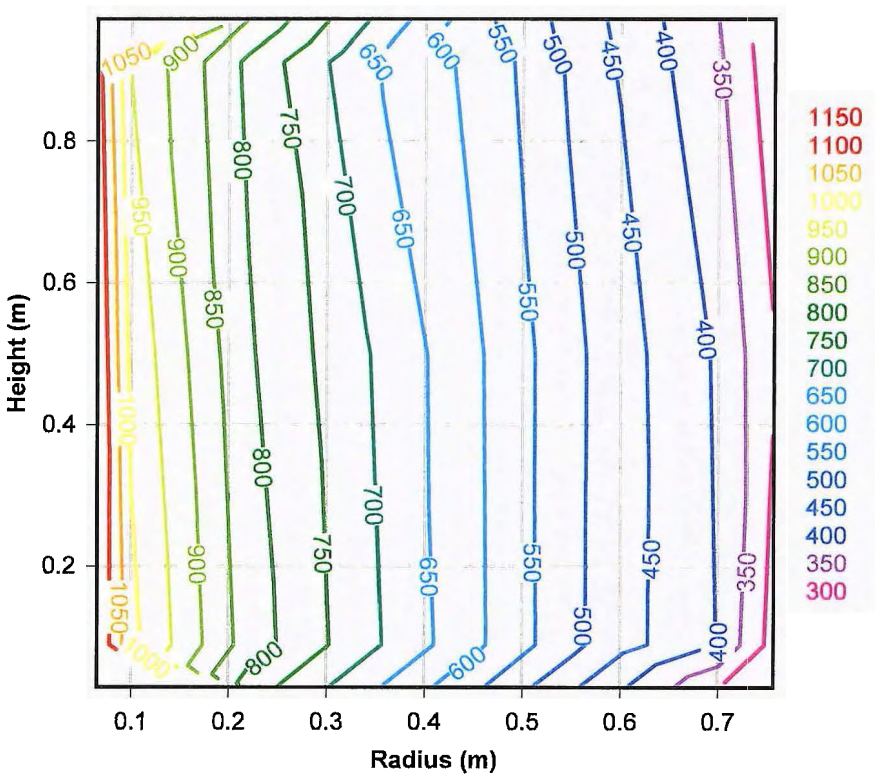

Figure C.5: Isothermal temperature distribution of SANA-I 35 kW helium steady-state at atmospheric pressure

Table C.12: Calculated effective thermal conductivity results for the 10 kW long heater element helium steady-state (SANA-I)

Wall region ↓ Wall region ↓

	RADIUS [m]						
	0.0825	0.16	0.28	0.40	0.52	0.64	0.728
HEIGHT [m]		Effective thermal conductivity [W/mK]					
0.91	7.924	9.639	10.120	7.794	6.202	7.619	2.480
0.5	5.989	9.895	11.647	8.405	7.146	8.889	4.042

Table C.13: Calculated effective thermal conductivity results for the 35 kW long heater element helium steady-state (SANA-I)

Wall region ↓ Wall region ↓

	RADIUS [m]						
	0.0825	0.16	0.28	0.40	0.52	0.64	0.728
HEIGHT [m]		Effective thermal conductivity [W/mK]					
0.91	16.262	21.260	19.808	13.754	10.011	11.015	3.296
0.5	13.636	22.199	21.749	14.812	10.362	10.305	4.358

Table C.14: Effective thermal conductivity data versus temperature (SANA-I) (Helium) (Niessen & Ball, 2000:306)

TEMP [°C]	k_eff [W/mK]	TEMP [°C]	k_eff [W/mK]
150	9	395	11.25
175	10	430	10.5
180	10.5	445	13
190	8.75	485	10.5
210	8.25	490	10
215	12.5	535	16
220	7	580	14.5
260	9.5	590	14
270	11.5	640	17.5
285	9	670	22
310	13	698	20
345	11.5	780	25
350	14.5	810	22.2
360	9.5	830	18.5
390	11		

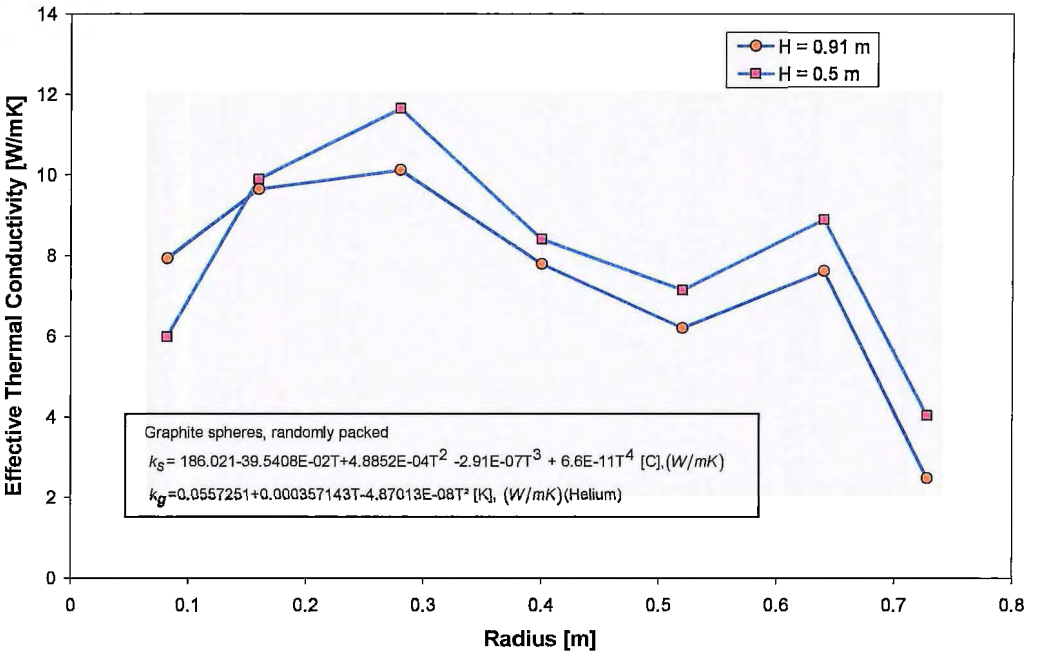

Figure C.6: Effective thermal conductivity results and other parameters for the 10 kW long heater element helium steady-state (SANA-I) at atmospheric pressure

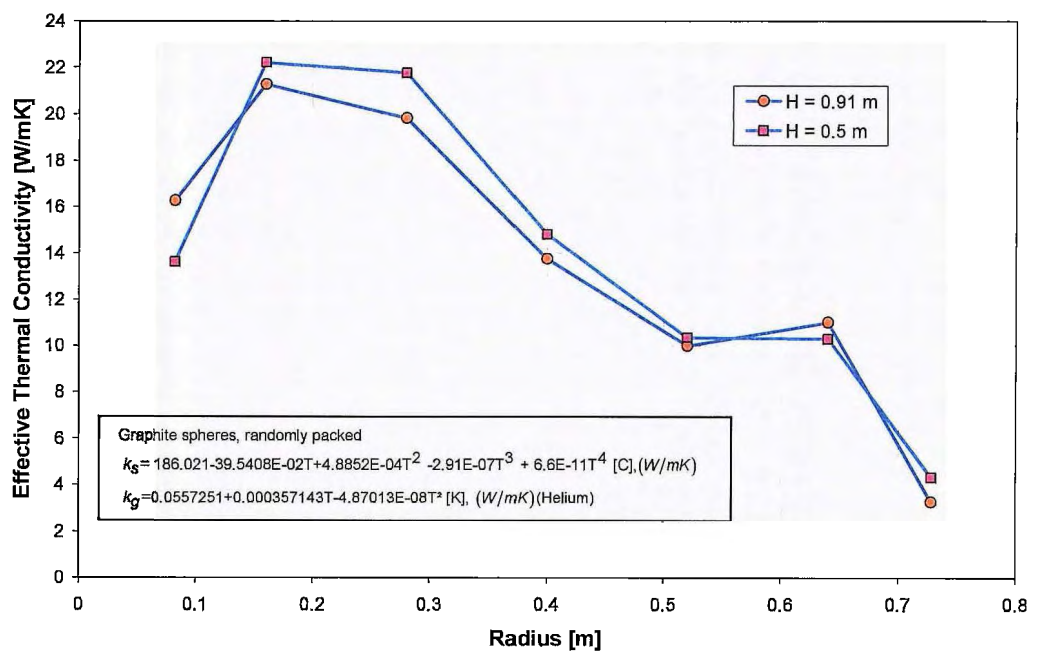

Figure C.7: Effective thermal conductivity results and other parameters for the 35 kW long heater element helium steady-state (SANA-I) at atmospheric pressure

APPENDIX D: HTTU ANALYSIS

This appendix provides an overview of several important aspects regarding the HTTU. It also presents relevant temperature and effective thermal conductivity results for various steady-states.

D.1 INSTRUMENT RANGE AND ACCURACY

Instruments that are of critical importance to the success of a test are referred to as category A instruments. Typically the results from these instruments are reported in the test report. Category B instruments are typically important for the operation of the plant but do not form part of the test results and follow a less stringent calibration schedule. Category C instruments are for indication purposes only (for instance the water level in the cooling tower) and are only checked/calibrated during commissioning. For this reason, only the instrument ranges and accuracies of category An instruments are listed in Table D.1.

Table D.1: Overview of category A ranges and accuracies

Component	Instrument range	Instrument accuracy
Annular packed bed		
Thermocouples in the bed		
Heat zone 1 (Type B)	Continuous: 100°C – 1600°C	± 5°C
	Short-term: 50°C – 1750°C	
Heat zone 2 (Type K)	Continuous: 0°C – 1100°C	± 3°C
	Short-term: -180°C – 1350°C	
Heat zone 3 (Type J)	Continuous: 20°C – 700°C	± 3°C
	Short-term: -80°C – 750°C	
Thermocouples in top & bottom insulation	0°C – 750°C	± 3°C
Water cooling		
Water jacket inlet temperature	0°C – 60°C	± 0.1 %
Water jacket outlet temperature	0°C – 100°C	± 0.1 %
Water jacket mass flow rate	0 – 5kg/s	± 0.5%
Stem coolers inlet & outlet temperature	0°C – 60°C	± 0.1 %
Stem coolers mass flow rate	0 – 1 kg/s	± 0.5%
Gas flow		
Vessel gas inlet temperature	0°C – 75°C	± 0.1 %
Vessel gas outlet temperature	0°C – 300°C	± 0.1 %
Orifice station temperature	0°C – 75°C	± 0.1 %
Pressure		
System absolute pressure	0 – 160 kPa (abs.)	± 0.25 %
System pressure differential	0 – 1 kPa	± 0.4%
Orifices upstream pressures	0 – 160 kPa (abs.)	± 0.25 %
Orifices differential pressures	0 – 1 kPa	± 0.4%

D.2 RADIAL HEAT FLUX DISTRIBUTION

A certain amount of the radial heat flux is lost through the top and bottom insulation of the HTTU $Q_{i,loss}(r)$ and varies with radial position, owing to the variation in the temperature and the heat transfer area through the insulation. Therefore, the heat flux through the bed $Q_{bed}(r)$ is also a function of radial position. The heat loss through the insulation was estimated by discretising the top and bottom insulation into forty equally spaced radial increments as displayed in Figure D.1. An estimated heat loss value was then calculated for each increment based on the measured bed and environmental temperatures. For each increment, the heat loss per unit length was calculated as follows:

$$Q_{i,loss} = \frac{k_{ins} A_i}{L_{ins}} (T_{bed} - T_{env}) \tag{D.1}$$

where $k_{ins} = 0.12[W/mK]$, $L_{ins} = 0.45m$, $T_{env} = (TE745K + TE750K)/2$ for the top insulation, with $TE745K$ and $TE750K$ specifically positioned thermocouples and $A_i = 2\pi\left(r_{i+1}^2 - r_i^2\right)$. The coldest bottom support plate temperature was taken as T_{env} in the calculations performed for the heat loss through the bottom insulation. The bed temperature was obtained by fitting a curve through the temperature measurements of Level A and Level E as shown in Figure D.2. The temperature T_{bed} was then obtained for the calculation in Eq. (D.1) at the radial position in the middle of the increment. The combined heat loss in the radial direction is shown in Figure D.3.

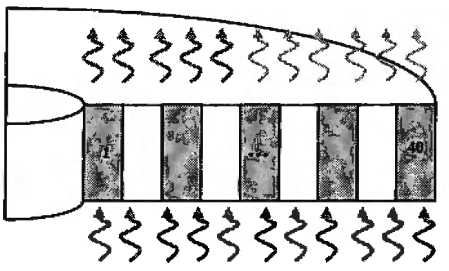

Figure D.1: Insulation discretisation of top insulation

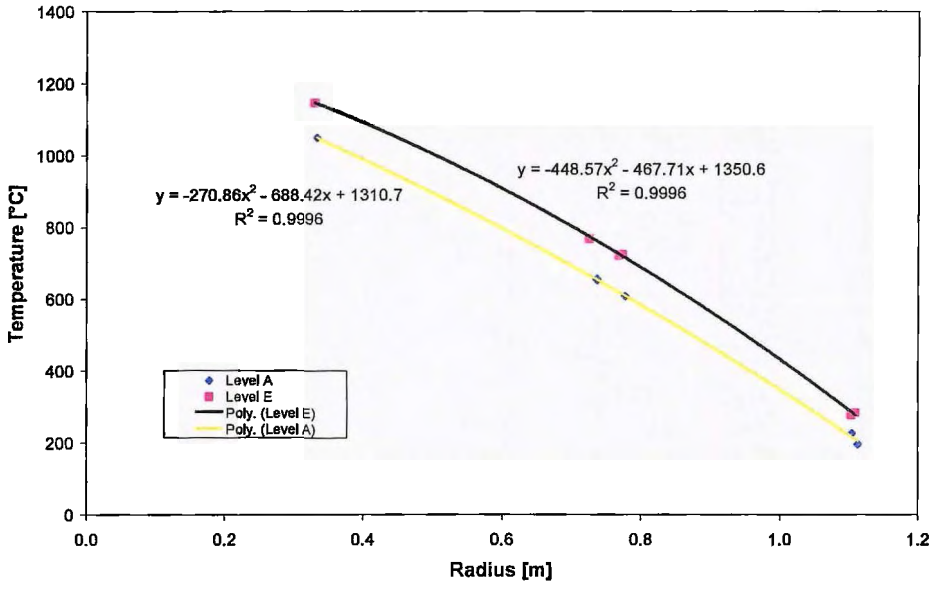

Figure D.2: Temperature curve fits for Level A and Level E (82.7 kW, Test 1)

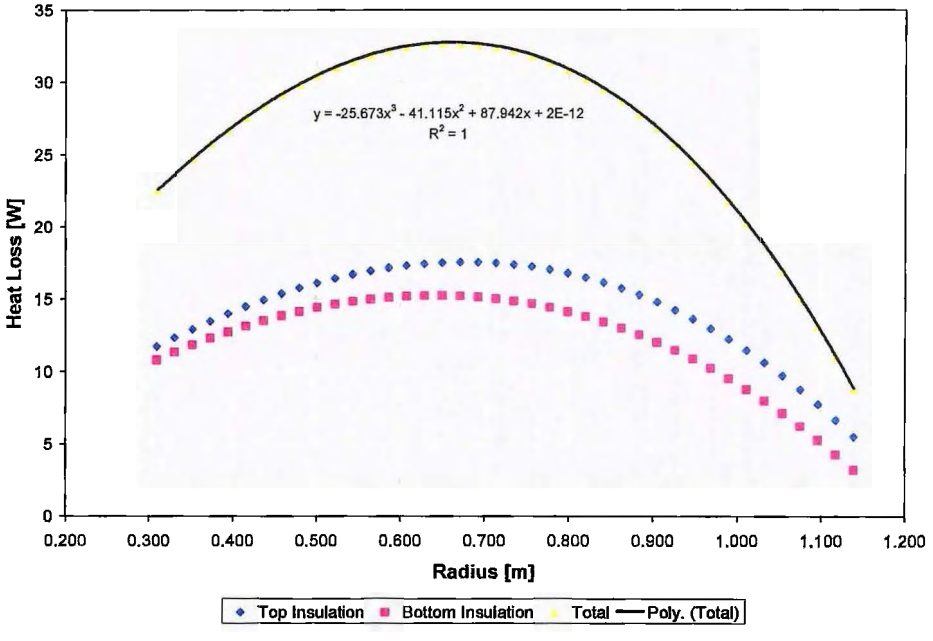

Figure D.3: Heat loss in each increment as a function of radial position

Again, a curve was fitted through the total heat loss, so that the following was obtained:

$$Q_{i,loss}(r_i) = -25.673r_i^3 - 41.115r_i^2 + 87.942r_i + 2\times10^{-12} \qquad \text{(D.2)}$$

The combined heat loss displayed in Eq. (D.1) was obtained for each steady-state and for each test. Therefore, the following relation was used to calculate the heat flux at a certain radial position increment :

$$Q_{bed}(r_j) = Q_{wj} + \left(Q_{total,loss} - \sum_{i=1}^{j-1} Q_{i,loss}(r_i) - Q_{j,loss}(r_j) \right) \tag{D.3}$$

where

$$Q_{total,loss} = \left(\sum_{i=1}^{40} Q_{i,loss,top\_insulation} + \sum_{i=1}^{40} Q_{i,loss,bottom\_insulation} \right)$$

The heat flux at the inner annulus wall r_{in} was taken as:

$$Q_{bed}(r_{in}) = Q_{wj} + \left(\sum_{i=1}^{40} Q_{i,loss,top\_insulation} + \sum_{i=1}^{40} Q_{i,loss,bottom\_insulation} \right) \tag{D.4}$$

and the heat flux at the outer annulus wall r_{out} was taken as:

$$Q_{bed}(r_{out}) = Q_{wj} \tag{D.5}$$

The radial heat flux as a function of radial position determined for the four steady-states is described by Eq.(D.6) with the coefficients for each case summarised in Table D.2:

$$Q_{bed}(r) = Q_{in} - \left[\frac{\left(c_0 + c_1 r + c_2 r^2 + c_3 r^3 \right)}{1000} \right] \tag{D.6}$$

where $Q_{bed}(r)$ is in $[kW]$, Q_{in} is the heat flux at $r_{in} = 0.3m$ and r in $[m]$, $(0.3m \le r \le 1.15m)$.

Table D.2: Heat flux distributions for various steady-states

	20kW Test 1	20kW Test 2	82.7 kW Test 1	82.7 kW Test 2
Q_{in}	12.215	11.975	66.377	67.241
c_0	-92.886	-85.297	-106.526	-102.567
c_1	134.569	78.705	-348.061	-364.285
c_2	773.211	897.097	2952.54	2963.63
c_3	-479.591	-537.006	-1532.44	-1535.62

D.3 UNCERTAINTY ANALYSIS

From Eq. (4.6) it can be seen that the uncertainty of two values need to be calculated i.e. uncertainty of the radial heat flux $u(Q_{bed})$ and uncertainty of the slope $u(dT/dr)$. The uncertainty of the radial heat flux $u(Q_{bed})$ consists of two components given as:

$$u(Q_{bed}) = \sqrt{u(Q_{wj})^2 + u(Q_{total,loss})^2} \tag{D.7}$$

where $u(Q_{wj})$ the uncertainty of the heat is extracted through the water jacket and $u(Q_{total,loss})$ is the uncertainty of the heat flux lost trough the top and bottom insulation.

The first component to be considered is $u(Q_{wj})$. The heat extracted by the water jacket was calculated as follows:

$$Q_{wj} = \dot{m} c_p (T_{we} - T_{wi}) \tag{D.8}$$

where the specific heat capacity c_p was taken at the average temperature $\bar{T}_{wj} = (T_{we} + T_{wi})/2$ and as a constant $c_p = 4.183 kJkg^{-1}K^{-1}$ due to the small temperature difference between the inlet and outlet water jacket temperatures that were $T_{wi} \approx 25°C$ and $T_{we} \approx 35°C$ respectively. The water jacket heat extraction uncertainty was then calculated as:

$$u(Q_{wj}) = \sqrt{\left[\left(\frac{\partial Q_{wj}}{\partial \dot{m}}\right) u(\dot{m})\right]^2 + \left[\left(\frac{\partial Q_{wj}}{\partial \Delta T_{wj}}\right) u(\Delta T_{wj})\right]^2} \tag{D.9}$$

The respected partial derivatives were calculated as follows:

$$\frac{\partial Q_{wj}}{\partial \dot{m}} = c_p \Delta T_{wj} \tag{D.10}$$

$$\frac{\partial Q_{wj}}{\partial \Delta T_{wj}} = \dot{m} c_p \tag{D.11}$$

where $u(\dot{m})$ is the statistical variance of the mass flow rate measurements. The uncertainty of the water jacket temperature difference $u(\Delta T_{wj})$ was calculated using the following:

$$u(\Delta T_{wj}) = \sqrt{\left[\left(\frac{\partial \Delta T_{wj}}{\partial T_{wi}}\right) \cdot u(T_{wi})\right]^2 + \left[\left(\frac{\partial \Delta T_{wj}}{\partial T_{we}}\right) \cdot u(T_{we})\right]^2} \tag{D.12}$$

The respective partial derivatives were calculated as follows:

$$\frac{\partial \Delta T_{wj}}{\partial T_{wi}} = -1 \tag{D.13}$$

$$\frac{\partial \Delta T_{wj}}{\partial T_{we}} = 1 \tag{D.14}$$

To calculate the uncertainty of the heat lost axially $u(Q_{total,loss})$ as displayed in Eq. (D.7), the uncertainty in each increment as displayed in Figure D.1 had to be considered first. This uncertainty $u(Q_{i,loss})$ was calculated for the top and bottom insulation by:

$$u(Q_{i,loss,top/bottom}) = \sqrt{\left(\frac{\partial Q_{i,loss}}{\partial T_{bed}} \cdot u(T_{bed})\right)^2 + \left(\frac{\partial Q_{i,loss}}{\partial T_{env}} \cdot u(T_{env})\right)^2} \quad (D.15)$$

The respective partial derivatives were calculated as follows:

$$\frac{\partial Q_{i,loss}}{\partial T_{bed}} = \frac{k_{ins} A_i}{L_{ins}} \quad (D.16)$$

$$\frac{\partial Q_{i,loss}}{\partial T_{env}} = -\frac{k_{ins} A_i}{L_{ins}} \quad (D.17)$$

For the environmental temperature uncertainty above the top insulation, the average of the two thermocouples in the gas environment was used, given by:

$$u(T_{env}) = \sqrt{\left(\frac{1}{2} \cdot u(TE745K)\right)^2 + \left(\frac{1}{2} \cdot u(TE750K)\right)^2} \quad (D.18)$$

where $u(TE745K)$ and $u(TE750K)$ were calculated by:

$$u(TE745K) = u(TE750K) = \sqrt{u(T_{i,statistical})^2 + u(T_{i,instrument})^2} \quad (D.19)$$

The environmental temperature uncertainty below the bottom insulation was obtained by considering the temperature measurement at the coldest part of the bottom support plate. It was chosen as such due to a lack of temperature measurements beneath the bottom. The uncertainty of the environmental temperature was then obtained as:

$$u(T_{env}) = \sqrt{u(T_{bottom\_sup,statistical})^2 + u(T_{bottom\_sup,instrument})^2} \quad (D.20)$$

The uncertainty $u(T_{bed})$ was obtained as follows:

$$u(T_{bed}) = \sqrt{u(T_{bed,statistical})^2 + u(T_{bed,instrument})^2 + u(SEE)^2} \quad (D.21)$$

where $u(T_{bed,statistical})$ is the maximum statistical variance of the top (level E) and bottom (level A) temperature measurements respectively. Also $u(T_{bed,instrument})$ is the maximum instrument uncertainty of the top (level E) and bottom (level A) thermocouples respectively. The maximum value is chosen in this calculation to be more conservative in the calculation of

$u(T_{bed})$. The uncertainty $u(SEE)$ is given by Dieck (2007:173) as the Standard Estimate Error (SEE). The SEE is a description and an estimate of the scatter of the data about a fitted line or curve, and is given by:

$$u(SEE) = \sqrt{\frac{\sum_{i=1}^{N}\left(T_{i,\exp} - T_{i,poly}\right)^2}{N-K}} \tag{D.22}$$

where $T_{i,\exp}$ is the i-th measurement in the experimental data set, $T_{i,poly}$ is the calculated value at r_i from the polynomial curve fitted, N the number data points in the experimental data set and K the number of coefficients in the polynomial equation.

Finally, the combined uncertainty of all the increments in the top and bottom insulation was obtained from:

$$u\left(Q_{total,loss}\right)_{top\_insulation} = \sqrt{u\left(Q_{1,loss,top}\right)^2 + \ldots + u\left(Q_{40,loss,top}\right)^2} \tag{D.23}$$

$$u\left(Q_{total,loss}\right)_{bottom\_insulation} = \sqrt{u\left(Q_{1,loss,bottom}\right)^2 + \ldots + u\left(Q_{40,loss,bottom}\right)^2} \tag{D.24}$$

Combining these total top and bottom uncertainties led to:

$$u\left(Q_{total,loss}\right) = \sqrt{u\left(Q_{total,loss}\right)^2_{top\_insulation} + u\left(Q_{total,loss}\right)^2_{bottom\_insulation}} \tag{D.25}$$

where $u\left(Q_{total,loss}\right)$ was used in Eq. (D.7).

The next component in Eq. (4.6) to calculate is the uncertainty of the slope $u(dT/dr)$. However, first to consider is the derivation of the polynomial curve fit through the data set as discussed by Van Antwerpen H.J. (2009:30). Suppose a function with the form as in Eq. (D.26), is fitted to a set of data (x_i, y_i).

$$y(x) = \sum_{k=0}^{m} a_k f_k(x) \tag{D.26}$$

where a_k are the coefficients associated with each function f_k. Eq. (D.26) can be written in matrix as:

$$y(x) = \begin{bmatrix} a_0 \\ a_1 \\ \vdots \\ a_m \end{bmatrix}^T \begin{bmatrix} f_0(x) \\ f_1(x) \\ \vdots \\ f_m(x) \end{bmatrix} = \underline{a}^T \underline{f} \tag{D.27}$$

In the case of a polynomial, the functions are as shown in Eq. (D.28), where m in Eq. (D.26) would be the order of the polynomial.

$$f_k(x) = x^k \tag{D.28}$$

The parameters a_0 to a_m are determined from the solution of the system of equations in Eq. (D.29), (Bevington & Robinson, 2003).

$$\underline{\beta} = \boldsymbol{\alpha}\underline{a}$$
$$\begin{bmatrix} \beta_0 \\ \beta_1 \\ \beta_2 \\ \beta_3 \\ \vdots \\ \beta_m \end{bmatrix} = \begin{pmatrix} \alpha_{00} & \cdots & \alpha_{0m} \\ \vdots & \ddots & \vdots \\ \alpha_{m0} & \cdots & \alpha_{mm} \end{pmatrix} \begin{bmatrix} a_0 \\ a_1 \\ a_2 \\ \vdots \\ a_m \end{bmatrix} \tag{D.29}$$

For a polynomial, the coefficients of $\underline{\beta}$ and α are calculated with Eq. (D.30), where N is the number of points in the data set.

$$\beta_k = \sum_i^N y_i x_i^k, \quad \alpha_{lk} = \sum_i^N x_i^l x_i^k \tag{D.30}$$

Let the inverse of the matrix α be given by ε so that

$$\underline{a} = \varepsilon\underline{\beta} \tag{D.31}$$

For a polynomial, the fitted function $y(x)$ is given by Eq. (D.32).

$$y(x) = \underline{\beta}^T \varepsilon^T \underline{f}(x)$$
$$\therefore y(x) = [\beta_0, \beta_1, \beta_2, \beta_3, \cdots, \beta_m] \begin{pmatrix} \varepsilon_{00} & \cdots & \varepsilon_{m0} \\ \vdots & \ddots & \vdots \\ \varepsilon_{0m} & \cdots & \varepsilon_{mm} \end{pmatrix} \begin{bmatrix} 1 \\ x \\ x^2 \\ \vdots \\ x^m \end{bmatrix} \tag{D.32}$$

The next to obtain is the uncertainty on the regression function. The variance in the fit at a point x, $u^2(x)$ is given by Eq.(D.33).

$$u^2(x) = \left(\frac{\partial y(x)}{\partial y_1}\right)^2 u_1^2 + \left(\frac{\partial y(x)}{\partial y_2}\right)^2 u_2^2 + \cdots + \left(\frac{\partial y(x)}{\partial y_N}\right)^2 u_N^2$$
$$u^2(x) = \sum_i^N \left(\frac{\partial y(x)}{\partial y_i}\right)^2 u_i^2 \tag{D.33}$$

The derivative in Eq. (D.33) is calculated by substituting the definition of $\underline{\beta}$ into Eq. (D.32) to

obtain Eq. (D.34)

$$\frac{\partial y(x)}{\partial y_i} = \left[1, x_i, x_i^2, \cdots, x_i^m\right] \begin{pmatrix} \varepsilon_{00} & \cdots & \varepsilon_{m0} \\ \vdots & \ddots & \vdots \\ \varepsilon_{0m} & \cdots & \varepsilon_{mm} \end{pmatrix} \begin{bmatrix} 1 \\ x \\ x^2 \\ \vdots \\ x^m \end{bmatrix} \tag{D.34}$$

Which can be rearranged to obtain Eq. (D.35)

$$\frac{\partial y(x)}{\partial y_i} = \left[1, x_i, x_i^2, \cdots, x_i^m\right] \begin{pmatrix} \varepsilon_{00} & +\varepsilon_{10}x & \cdots & +\varepsilon_{m0}x^m \\ \varepsilon_{01} & +\varepsilon_{11}x & & +\varepsilon_{m1}x^m \\ & \vdots & & \vdots \\ \varepsilon_{0m} & +\varepsilon_{1m}x & \cdots & +\varepsilon_{mm}x^m \end{pmatrix} \tag{D.35}$$

Due to the rules of matrix multiplication, it is possible to arrange Eq. (D.35) as shown in Eq. (D.36).

$$\frac{\partial y(x)}{\partial y_i} = \left[1, x_i, x_i^2, \cdots, x_i^m\right] \begin{pmatrix} \sum_{j=0}^{m} \varepsilon_{0j} x^j \\ \vdots \\ \sum_{j=0}^{m} \varepsilon_{mj} x^j \end{pmatrix} \tag{D.36}$$

$$\frac{\partial y(x)}{\partial y_i} = \sum_{k=0}^{m} \left(x_i^k \sum_{j=0}^{m} \varepsilon_{kj} x^j \right)$$

Substitute Eq. (D.36) in Eq. (D.33) to obtain Eq. (D.37)

$$u^2(x) = \sum_{i}^{N} \left(\sum_{k=0}^{m} \left(x_i^k \sum_{j=0}^{m} \varepsilon_{kj} x^j \right) \right)^2 u_i^2 \tag{D.37}$$

The data point uncertainty is the sum of the measurement uncertainty and the scatter uncertainty, which is the difference between the curve fit and the data point, as shown in Eq. (D.38).

$$\begin{aligned} u_i^2 &= u_{meas,i}^2 + u_{scatter,i}^2 \\ &= u_{meas,i}^2 + \left| y(x) - y_i \right|^2 \end{aligned} \tag{D.38}$$

Instrument, drift and statistical variance are all included in the measurement uncertainty, similar to Eq. (4.5).

With the uncertainty in the data point known one must calculate the uncertainty in the derivative (slope) of the regression polynomial. Again this is adopted from Van Antwerpen H.J. (2009:32).

The derivative or slope $a(x)$ of the regression polynomial $y(x)$ is found by differentiating Eq. (D.32), as shown in Eq. (D.39)

$$a(x)=\frac{dy(x)}{dx}=\frac{d}{dx}\left[\left[\beta_0,\beta_1,\beta_2,\beta_3,\cdots,\beta_m\right]\begin{pmatrix}\varepsilon_{00} & \cdots & \varepsilon_{m0}\\ \vdots & \ddots & \vdots\\ \varepsilon_{0m} & \cdots & \varepsilon_{mm}\end{pmatrix}\begin{bmatrix}1\\ x\\ x^2\\ \vdots\\ x^m\end{bmatrix}\right]$$
$$=\left[\beta_0,\beta_1,\beta_2,\beta_3,\cdots,\beta_m\right]\begin{pmatrix}\varepsilon_{00} & \cdots & \varepsilon_{m0}\\ \vdots & \ddots & \vdots\\ \varepsilon_{0m} & \cdots & \varepsilon_{mm}\end{pmatrix}\begin{bmatrix}0\\ 1\\ 2x\\ 3x^2\\ \vdots\\ mx^{m-1}\end{bmatrix}. \tag{D.39}$$

The uncertainty in the slope $a(x)$ is then given by Eq. (D.40).

$$\sigma^2\left(a(x)\right)=\sum_i^N\left(\frac{\partial a(x)}{\partial y_i}\right)^2\sigma_i^2 \tag{D.40}$$

Similar to the procedure followed for the uncertainty in $y(x)$, the derivative $\frac{\partial a(x)}{\partial y_i}$ is calculated in Eq. (D.41).

$$\frac{\partial a(x)}{\partial y_i}=\left[1,x_i,x_i^2,\cdots,x_i^m\right]\begin{pmatrix}\varepsilon_{00} & \cdots & \varepsilon_{m0}\\ \vdots & \ddots & \vdots\\ \varepsilon_{0m} & \cdots & \varepsilon_{mm}\end{pmatrix}\begin{bmatrix}0\\ 1\\ 2x\\ 3x^2\\ \vdots\\ mx^{m-1}\end{bmatrix} \tag{D.41}$$

This can be rearranged to obtain Eq. (D.42)

$$\frac{\partial a(x)}{\partial y_i}=\left[1,x_i,x_i^2,\cdots,x_i^m\right]\begin{pmatrix}\varepsilon_{01}+\varepsilon_{20}2x & & +\varepsilon_{m0}mx^{m-1}\\ \varepsilon_{11}+\varepsilon_{21}2x & \cdots & +\varepsilon_{m1}mx^{m-1}\\ \varepsilon_{12}+\varepsilon_{22}2x & & +\varepsilon_{m2}mx^{m-1}\\ \vdots & & \vdots\\ \varepsilon_{1m}+\varepsilon_{2m}2x & \cdots & +\varepsilon_{mm}mx^{m-1}\end{pmatrix} \tag{D.42}$$

Due to the rules of matrix multiplication, it is possible to arrange Eq. (D.42) as shown in Eq. (D.43).

$$\frac{\partial a(x)}{\partial y_i} = \left[1, x_i, x_i^2, \cdots, x_i^m\right] \begin{pmatrix} \sum_{j=1}^{m} \varepsilon_{0j} j x^{j-1} \\ \vdots \\ \sum_{j=1}^{m} \varepsilon_{mj} j x^{j-1} \end{pmatrix} \qquad \text{(D.43)}$$

$$\frac{\partial a(x)}{\partial y_i} = \sum_{k=0}^{m} \left(x_i^k \sum_{j=1}^{m} \varepsilon_{kj} j x^{j-1} \right)$$

Substitute Eq. (D.43) in Eq. (D.40) to obtain Eq. (D.44)

$$\sigma^2(x) = \sum_{i}^{N} \left(\sum_{k=0}^{m} \left(x_i^k \sum_{j=1}^{m} \varepsilon_{kj} j x^{j-1} \right) \right)^2 \sigma_i^2 \qquad \text{(D.44)}$$

Thus, Eq. (D.44) gives the uncertainty in the slope of the fitted curve as a function of x. Note that Eq. (D.44) retains the locality of the input uncertainty information, while simultaneously taking into account the effect of all the other input data points on the local uncertainty. Ultimately, the following can be written to be substituted into Eq. (4.6):

$$u\left(\frac{dT}{dr}(r)\right) = \sigma(x) \qquad \text{(D.45)}$$

D.4 TEMPERATURE AND EFFECTIVE THERMAL CONDUCTIVITY RESULTS

This section summarises the relevant temperature measurements and the extracted effective thermal conductivity results. Temperature measurements with their standard deviation are shown for the various steady-state tests in Table D.3 and Table D.4. The extracted effective thermal conductivities for all the tests are shown in Table D.5 to Table D.9.

Table D.3: Temperature measurements for both tests on Level C for the 20 kW steady-state

TEST 1 LEVEL C			TEST 2 LEVEL C		
Radius (m)	Temp. (°C)	Uncertainty (°C)	Radius (m)	Temp. (°C)	Uncertainty (°C)
0.300	544.20	3.442	0.300	553.68	3.442
0.300	545.14	3.453	0.300	559.81	3.444
0.300	555.71	3.442	0.300	557.91	3.443
0.300	548.55	3.442	0.330	523.91	3.451
0.300	549.24	3.452	0.330	526.29	3.450
0.330	513.91	3.451	0.338	539.54	3.453
0.330	517.51	3.451	0.377	493.71	3.451
0.338	529.43	3.455	0.383	496.64	3.452
0.377	483.08	3.455	0.437	455.55	3.457
0.383	490.99	3.456	0.442	459.32	3.453
0.437	442.45	3.455	0.451	448.61	3.453
0.442	447.30	3.452	0.494	420.14	3.452
0.451	433.57	3.456	0.521	403.43	3.461
0.494	405.23	3.457	0.571	383.17	3.464
0.521	388.98	3.460	0.616	348.13	5.762
0.571	368.03	3.471	0.618	346.56	5.762
0.616	332.92	5.762	0.666	326.99	5.762
0.618	330.16	5.762	0.674	317.62	5.762
0.666	310.30	5.762	0.688	308.89	5.762
0.674	302.24	5.762	0.720	281.95	5.762
0.688	296.26	5.762	0.752	274.09	5.762
0.720	266.58	5.762	0.758	267.29	5.762
0.752	255.40	5.762	0.775	252.15	5.762
0.758	254.30	5.762	0.795	247.44	5.762
0.775	238.41	5.762	0.820	238.00	6.269
0.795	232.93	5.762	0.824	226.16	5.762
0.820	228.41	6.257	0.842	221.51	5.762
0.824	213.62	5.762	0.874	200.37	5.762
0.842	206.84	5.762	0.896	190.75	5.762
0.874	190.85	5.762	0.931	172.98	5.762
0.896	176.10	5.762	0.932	172.25	5.762
0.931	156.96	5.762	0.955	158.90	3.603
0.932	158.48	5.762	0.967	154.54	3.603
0.955	151.49	3.603	0.992	146.64	3.603
0.967	143.22	3.603	1.022	126.42	3.603
0.992	138.43	3.603	1.025	122.71	3.603
1.022	117.14	3.603	1.052	108.91	3.603
1.025	115.72	3.603	1.079	91.13	3.603

TEST 1 LEVEL C			TEST 2 LEVEL C		
Radius (m)	Temp. (°C)	Uncertainty (°C)	Radius (m)	Temp. (°C)	Uncertainty (°C)
1.052	102.11	3.603	1.084	85.49	3.603
1.079	83.82	3.603	1.103	73.18	3.603
1.084	81.25	3.603	1.150	44.31	3.603
1.103	70.04	3.603	1.150	43.07	3.603
1.150	43.63	3.603	1.150	48.73	3.603
1.150	42.48	3.603	1.150	48.90	3.603
1.150	47.39	3.603	1.150	46.49	3.603
1.150	47.46	3.603	1.150	46.26	3.603
1.150	45.60	3.603			
1.150	45.44	3.603			

Table D.4: Temperature measurements for both tests on Level C for the 82.7 kW steady-state

TEST 1 LEVEL C			TEST 2 LEVEL C		
Radius (m)	Temp. (°C)	Uncertainty (°C)	Radius (m)	Temp. (°C)	Uncertainty (°C)
0.300	1182.10	3.442	0.300	1167.88	3.442
0.300	1187.88	3.442	0.300	1179.22	3.442
0.300	1182.36	3.442	0.300	1176.17	3.442
0.330	1124.23	3.445	0.330	1121.55	3.445
0.330	1130.58	3.445	0.330	1129.20	3.445
0.338	1130.10	3.445	0.338	1128.67	3.446
0.377	1076.09	3.445	0.377	1075.03	3.445
0.383	1079.77	3.459	0.383	1071.95	3.469
0.437	1020.88	3.445	0.437	1018.82	3.446
0.442	1019.30	3.445	0.442	1018.05	3.445
0.451	1013.30	3.445	0.451	1012.49	3.445
0.494	970.12	3.445	0.494	968.63	3.445
0.521	943.77	3.444	0.507	982.08	3.446
0.563	911.83	3.445	0.521	943.39	3.446
0.571	902.73	3.445	0.563	921.02	3.447
0.616	844.78	5.762	0.571	902.29	3.446
0.618	848.65	5.762	0.616	844.44	5.762
0.666	807.67	5.762	0.618	848.73	5.762
0.674	796.50	5.762	0.666	807.98	5.762
0.688	786.04	5.762	0.674	795.32	5.762
0.720	739.92	5.762	0.688	784.50	5.762
0.752	715.72	5.762	0.720	739.95	5.762
0.758	717.09	5.762	0.752	716.14	5.762
0.775	687.09	5.762	0.758	714.96	5.762
0.795	675.62	5.762	0.775	685.90	5.762
0.824	635.76	5.762	0.795	675.58	5.762
0.842	620.92	5.762	0.824	633.90	5.762
0.874	590.83	5.762	0.842	621.19	5.762
0.896	555.44	5.762	0.874	588.52	5.762
0.931	514.88	5.762	0.896	553.51	5.762
0.932	528.48	5.762	0.931	514.92	5.762
0.955	487.59	3.603	0.932	525.55	5.762
0.967	466.13	3.603	0.955	487.00	3.603
0.992	455.96	3.603	0.967	465.68	3.603

TEST 1 LEVEL C			TEST 2 LEVEL C		
Radius (m)	Temp. (°C)	Uncertainty (°C)	Radius (m)	Temp. (°C)	Uncertainty (°C)
1.022	383.07	3.603	0.992	452.33	3.603
1.025	380.81	3.603	1.022	382.31	3.603
1.052	347.09	3.603	1.025	378.01	3.603
1.079	296.37	3.603	1.052	343.57	3.603
1.084	270.29	3.603	1.079	290.08	3.603
1.103	226.58	3.603	1.084	267.62	3.603
1.150	99.31	3.603	1.103	225.77	3.603
1.150	94.99	3.603	1.150	98.49	3.603
1.150	107.74	3.603	1.150	94.31	3.603
1.150	106.85	3.603	1.150	107.04	3.603
1.150	102.70	3.603	1.150	106.55	3.603
1.150	101.65	3.603	1.150	102.14	3.603
			1.150	100.97	3.603

Table D.5: Effective thermal conductivity extracted values for Test 1 on Level C for the 20 kW steady-state

Radius (m)	Sphere diameter	T	u(T)	k_eff	u(k_eff)
0.300	0.000	548.202	2.457	6.237	0.710
0.360	1.000	499.952	2.814	5.973	0.375
0.420	2.000	457.187	2.685	5.642	0.354
0.480	3.000	417.762	2.147	5.249	0.354
0.540	4.000	380.295	2.203	4.841	0.304
0.600	5.000	344.017	2.418	4.463	0.259
0.660	6.000	308.618	2.322	4.144	0.247
0.730	7.167	268.439	2.056	3.858	0.243
0.790	8.167	235.140	2.075	3.682	0.229
0.850	9.167	203.046	2.178	3.548	0.210
0.910	10.167	172.125	2.021	3.423	0.211
0.970	11.167	142.022	1.698	3.259	0.223
1.030	12.167	111.901	1.778	3.002	0.200
1.090	13.167	80.295	1.826	2.623	0.168
1.150	14.167	44.955	1.648	2.149	0.259

Table D.6: Effective thermal conductivity extracted values for Test 1 on Level D for the 20 kW steady-state

Radius (m)	Sphere diameter	T	u(T)	k_eff	u(k_eff)
0.300	0.000	573.703	3.421	5.404	0.578
0.360	1.000	521.300	2.420	5.830	0.396
0.420	2.000	479.142	2.414	5.900	0.371
0.480	3.000	441.860	2.216	5.568	0.364
0.540	4.000	406.210	2.309	5.020	0.306
0.600	5.000	370.620	2.346	4.471	0.258
0.660	6.000	334.761	2.095	4.039	0.241
0.730	7.167	293.229	1.789	3.720	0.231
0.790	8.167	258.826	1.865	3.588	0.217
0.850	9.167	226.250	1.979	3.538	0.207
0.910	10.167	195.572	1.812	3.477	0.220
0.970	11.167	165.818	1.669	3.255	0.230
1.030	12.167	134.529	2.123	2.752	0.180
1.090	13.167	97.320	2.321	2.052	0.123
1.150	14.167	47.437	1.681	1.387	0.126

Table D.7: Effective thermal conductivity extracted values for Test 2 on Level C for the 20 kW steady-state

Radius (m)	Sphere diameter	T	u(T)	k_eff	u(k_eff)
0.300	0.000	556.462	2.837	6.258	0.655
0.360	1.000	509.811	2.623	6.110	0.361
0.420	2.000	468.990	2.310	5.802	0.347
0.480	3.000	431.327	1.897	5.362	0.339
0.540	4.000	395.139	2.124	4.874	0.281
0.600	5.000	359.533	2.381	4.416	0.235
0.660	6.000	324.206	2.287	4.035	0.221
0.730	7.167	283.476	2.005	3.700	0.215
0.790	8.167	249.309	1.978	3.496	0.199
0.850	9.167	216.102	2.031	3.344	0.182
0.910	10.167	183.877	1.854	3.201	0.182
0.970	11.167	152.215	1.569	3.013	0.188
1.030	12.167	120.067	1.719	2.724	0.164
1.090	13.167	85.547	1.806	2.316	0.135
1.150	14.167	45.738	1.713	1.836	0.191

Table D.8: Effective thermal conductivity extracted values for Test 1 on Level C for the 82.7 kW steady-state

Radius (m)	Sphere diameter	T	u(T)	k_eff	u(k_eff)
0.300	0.000	1180.267	3.390	18.908	1.446
0.360	1.000	1100.334	2.593	21.157	1.101
0.420	2.000	1037.592	2.296	21.674	1.122
0.480	3.000	981.917	1.931	20.135	1.085
0.540	4.000	927.234	2.271	17.574	0.880
0.600	5.000	870.585	2.574	15.077	0.718
0.660	6.000	811.203	2.489	13.096	0.636
0.730	7.167	739.157	2.295	11.440	0.568
0.790	8.167	675.942	2.406	10.377	0.509
0.850	9.167	611.458	2.588	9.378	0.455
0.910	10.167	544.064	2.661	8.184	0.408
0.970	11.167	469.510	2.916	6.678	0.336
1.030	12.167	380.003	3.431	5.019	0.240
1.090	13.167	263.286	3.176	3.515	0.168
1.150	14.167	101.703	2.318	2.361	0.132

Table D.9: Effective thermal conductivity extracted values for Test 2 on Level C for the 82.7 kW steady-state

Radius (m)	Sphere diameter	T	u(T)	k_eff	u(k_eff)
0.300	0.000	1171.466	3.552	21.055	1.804
0.360	1.000	1098.036	2.524	23.031	1.308
0.420	2.000	1038.769	2.793	22.869	1.235
0.480	3.000	984.520	2.982	20.653	1.124
0.540	4.000	929.970	3.312	17.705	0.887
0.600	5.000	872.723	3.331	15.062	0.726
0.660	6.000	812.407	2.909	13.052	0.648
0.730	7.167	739.188	2.373	11.414	0.578
0.790	8.167	675.070	2.387	10.380	0.513
0.850	9.167	609.861	2.589	9.412	0.452
0.910	10.167	541.954	2.611	8.245	0.404
0.970	11.167	467.128	2.695	6.755	0.337
1.030	12.167	377.644	3.104	5.096	0.243
1.090	13.167	261.346	2.923	3.579	0.170
1.150	14.167	100.767	2.705	2.410	0.135

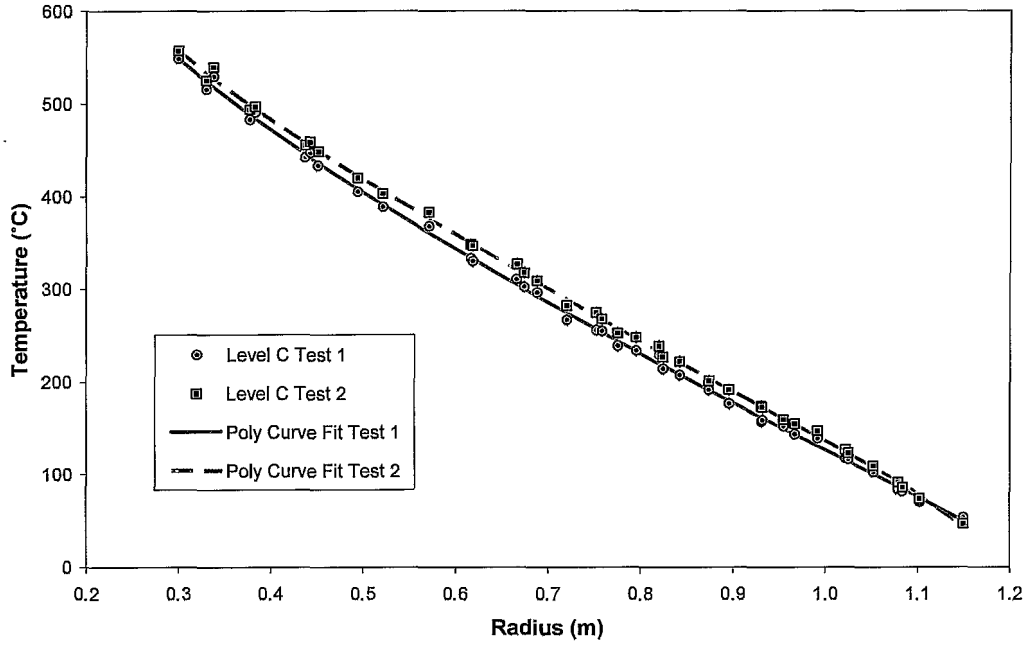

Figure D.4: Temperature profile of level C (20 kW steady-state)

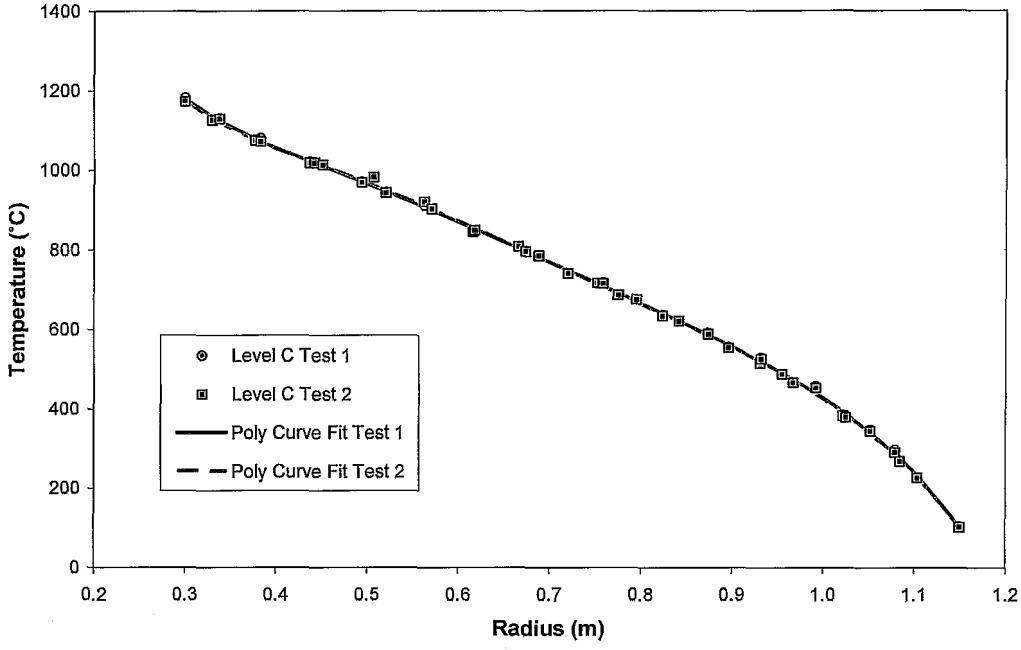

Figure D.5: Temperature profile of level C (82.7 kW steady-state)

D.5 CONTACT FORCE DISTRIBUTION

The same numerically packed bed data set used for calculating the radial porosity, coordination number and contact angles are used to calculate the average contact force on each pebble as a function of pebble bed depth. Polson (2006) who generated the numerically packed bed treats the contact region as two springs that compresses against each other (Figure D.6). It was experimentally found by Polson (2006) that the spring stiffness for the HTTU graphite sphere results in a linear relationship and found the spring stiffness to be $k_1 = k_2 = 15000\ kN/m$. The combined stiffness between two spheres can be calculated by:

$$k = \frac{k_1 k_2}{k_1 + k_2} \tag{D.46}$$

where k is the combined stiffness between sphere one and two. The deformation depth ω_0 can be calculated using:

$$\omega_0 = d_p - d_F \tag{D.47}$$

where d_p is the pebble diameter and $d_F = d_p - \omega_0$ the distance between the two pebble centres due to an external force acting on the pebbles. The contact force can then be calculated by:

$$F = \omega_0 k \tag{D.48}$$

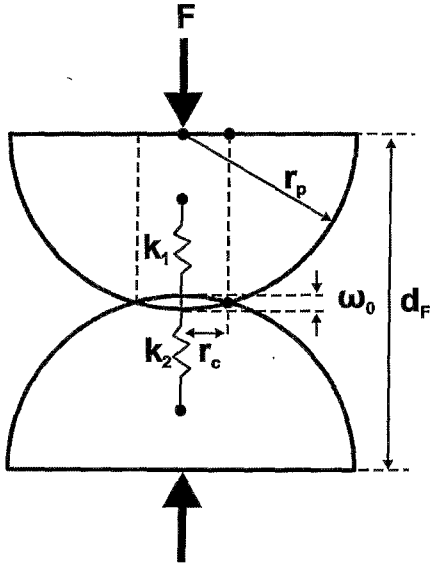

Figure D.6: Spring representation of contact force calculations

The distance between spheres in contact for the numerically packed bed was calculated using the C++ program presented in Appendix G.1. The contact force between each pebble was then further calculated in an Excel sheet. The first analysis done was to determine if the

wall has an effect on the contact force distribution. Portions of the bed (100mm) were taken and averages calculated with pebbles falling inside a radial slide with a thickness of $1/4d_p$. The result is presented in Figure D.7. From Figure D.7 no real distinction can be seen between the near-wall and the bulk region.

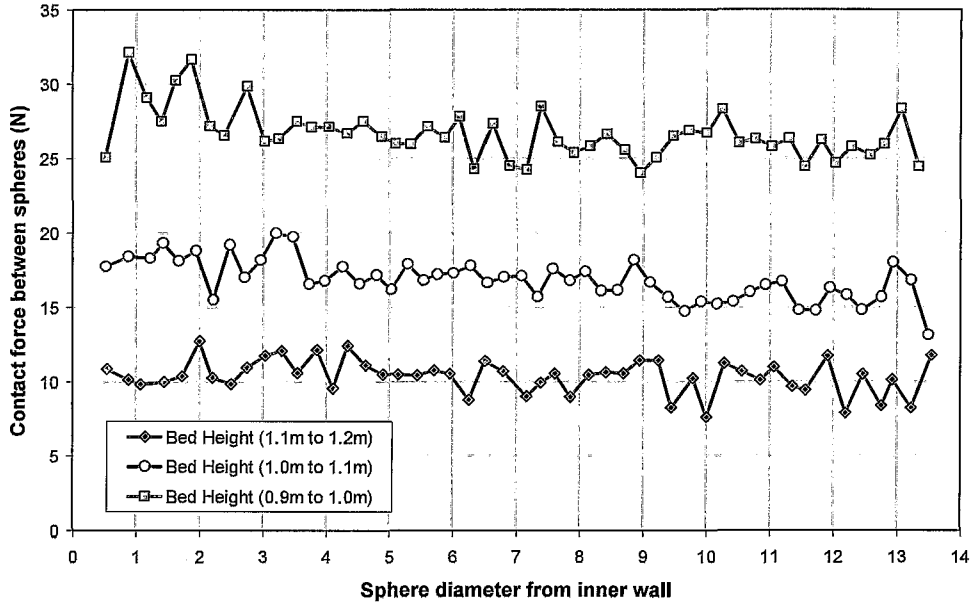

Figure D.7: Contact force radial distribution for different height portions in HTTU

A further analysis was done calculating an average contact force as a function of depth. This was achieved by calculating an average contact force for pebble centres falling in increments of $1/4d_p$ increasing in height. The result is presented in Figure D.8 and a linear curve fit was obtained given by:

$$F = 72.307 \cdot Z_{depth} + 7.8716 \tag{D.49}$$

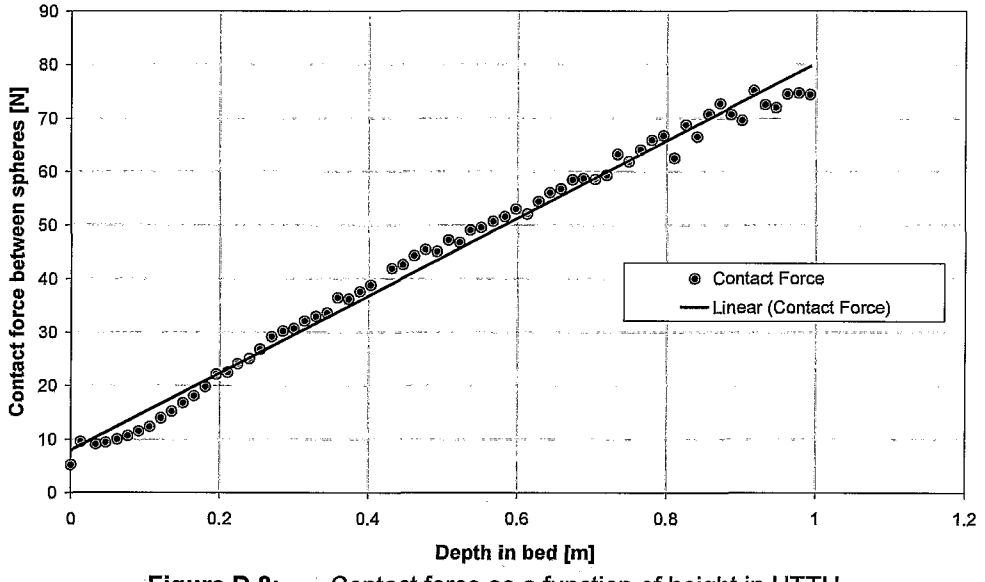

Figure D.8: Contact force as a function of height in HTTU

APPENDIX E: INTEGRATION PROCESSES OF MULTI-SPHERE UNIT CELL

This appendix presents the integration processes of several thermal resistances derived in this study.

BULK REGION:

THERMAL RESISTANCE OF THE INTERSTITIAL GAS IN THE SMOLUCHOWSKI REGIME:

The thermal resistance of the interstitial gas in the Knudsen regime (Smoluchowski effect) of the macrogap R_λ is derived by the procedure displayed below. The integration parameter displayed in Eq. (5.21) is:

$$2\pi k_g R_\lambda = \left[\int_{a_L}^{r_\lambda} \frac{r}{2r_p - \omega_0 - 2\sqrt{r_p^2 - r^2} + j}\,dr\right]^{-1} \tag{E.1}$$

If $A_\lambda = 2r_p + j - \omega_0$, the indefinite integral is given as:

$$\int \frac{x}{a - b\sqrt{c^2 - x^2}}\,dx = \frac{a\ln\left|a - b\sqrt{c^2 - x^2}\right|}{b^2} + \frac{\sqrt{c^2 - x^2}}{b} \tag{E.2}$$

Thus:

$$\int_{a_L}^{r_\lambda} \frac{r\,dr}{A_\lambda - 2\sqrt{r_p^2 - r^2}} = \left[\frac{A_\lambda \ln\left|A_\lambda - 2\sqrt{r_p^2 - r^2}\right|}{4} + \frac{\sqrt{r_p^2 - r^2}}{2}\right]_{a_L}^{r_\lambda} \tag{E.3}$$

$$= \frac{A_\lambda \ln\left|A_\lambda - 2\sqrt{r_p^2 - r_\lambda^2}\right|}{4} + \frac{\sqrt{r_p^2 - r_\lambda^2}}{2} - \frac{A_\lambda \ln\left|A_\lambda - 2\sqrt{r_p^2 - a_L^2}\right|}{4} - \frac{\sqrt{r_p^2 - a_L^2}}{2} \tag{E.4}$$

If $B_\lambda = \sqrt{r_p^2 - r_\lambda^2}$ and $C_\lambda = \sqrt{r_p^2 - a_L^2}$:

$$= \frac{A_\lambda}{4}\left(\ln\left|A_\lambda - 2B_\lambda\right| - \ln\left|A_\lambda - 2C_\lambda\right|\right) + \frac{B_\lambda}{2} - \frac{C_\lambda}{2} \tag{E.5}$$

$$= \frac{1}{4}\left[A_\lambda \left(\ln \left| \frac{A_\lambda - 2B_\lambda}{A_\lambda - 2C_\lambda} \right| \right) + 2B_\lambda - 2C_\lambda \right] \tag{E.6}$$

Substituting Eq. (E.6) into Eq. (E.1) yields:

$$R_\lambda = \frac{2}{\pi k_g \left(A_\lambda \left(\ln \left| \frac{A_\lambda - 2B_\lambda}{A_\lambda - 2C_\lambda} \right| \right) + 2B_\lambda - 2C_\lambda \right)} \tag{E.7}$$

THERMAL RESISTANCE OF THE INTERSTITIAL GAS IN THE MACRO GAP:

The integral of the thermal resistance in the interstitial gas situated in the macrogap R_G is derived as follows:

The integration parameter displayed in Eq. (5.26) is:

$$R_G = \frac{1}{2\pi k_g} \left[\int_{r_\lambda}^{r_p} \frac{r}{2r_p - \omega_0 - 2\sqrt{r_p^2 - r^2}} dr \right]^{-1} \tag{E.8}$$

If $A_G = 2r_p - \omega_0$, the indefinite integral is given by Eq. (E.2), thus:

$$\int_{r_\lambda}^{r_p} \frac{r dr}{A_G - 2\sqrt{r_p^2 - r^2}} = \left[\frac{A_G \ln \left| A_G - 2\sqrt{r_p^2 - r^2} \right|}{4} + \frac{\sqrt{r_p^2 - r^2}}{2} \right]_{r_\lambda}^{r_p} \tag{E.9}$$

$$= \frac{A_G \ln \left| A_G - 2\sqrt{r_p^2 - r_p^2} \right|}{4} + \frac{\sqrt{r_p^2 - r_p^2}}{2} - \frac{A_G \ln \left| A_G - 2\sqrt{r_p^2 - r_\lambda^2} \right|}{4} - \frac{\sqrt{r_p^2 - r_\lambda^2}}{2} \tag{E.10}$$

If $B_G = \sqrt{r_p^2 - r_\lambda^2}$, then:

$$= \frac{A_G}{4} \left(\ln |A_G| - \ln |A_G - 2B_G| \right) - \frac{B_G}{2} \tag{E.11}$$

$$= \frac{1}{4}\left[A_G \left(\ln \left| \frac{A_G}{A_G - 2B_G} \right| \right) - 2B_G \right] \tag{E.12}$$

Substituting Eq. (E.12) into Eq. (E.8) yields:

$$R_G = \frac{2}{\pi k_g \left(A_G \left(\ln \left| \frac{A_G}{A_G - 2B_G} \right| \right) - 2B_G \right)} \tag{E.13}$$

THERMAL RESISTANCE OF THE OUTER SOLID REGION:

The bulk outer solid resistance $R_{out,1,2}$ is derived by the following procedure:

The integration parameter displayed in Eq. (5.31) is:

$$\frac{Q_y}{k_s \pi} \int_0^{r_p - 2L_{out}} \frac{1}{\left(r_p^2 - r_\lambda^2 - y^2 \right)} \partial y = -\int_{T_2}^{T_1} \partial T \tag{E.14}$$

where $L_{out} = \left(0.5\omega_0 + 5\lambda\right)$ with T_1 the temperature in the centre of the pebble and T_2 the temperature at a distance $2L_{out}$ from the origin in the y direction, as displayed in Figure 5.3.

The indefinite integral is given as:

$$\int \frac{1}{a^2 - b^2 - y^2} dy = \frac{\ln\left| y + \sqrt{a-b}\sqrt{b+a} \right| - \ln\left| y - \sqrt{a-b}\sqrt{b+a} \right|}{2\sqrt{a-b}\sqrt{b+a}} \tag{E.15}$$

Thus:

$$\int_0^{r_p - 2L_{out}} \frac{1}{r_p^2 - r_\lambda^2 - y^2} dy = \frac{Q_y}{k_s \pi} \left[\frac{\ln \left| \frac{y + \sqrt{r_p^2 - r_\lambda^2}}{y - \sqrt{r_p^2 - r_\lambda^2}} \right|}{2\sqrt{r_p^2 - r_\lambda^2}} \right]_0^{r_p - 2L_{out}} \tag{E.16}$$

If $A_{out} = r_p - 2L_{out} = r_p - 2\left(0.5\omega_0 + 5\lambda\right)$ and $B_{out} = \sqrt{r_p^2 - r_\lambda^2}$, then the thermal resistance in the outer bulk solid region for one sphere is:

$$R_{out,1} = \frac{\ln \left| \frac{A_{out} + B_{out}}{A_{out} - B_{out}} \right|}{2k_s \pi B_{out}} \tag{E.17}$$

where r_λ is the mean free-path radius, defined in Eq. (5.17).

However, the thermal resistance for both spheres is:

$$R_{out,1,2} = \frac{\ln\left|\frac{A_{out}+B_{out}}{A_{out}-B_{out}}\right|}{k_s \pi B_{out}} \tag{E.18}$$

WALL REGION:

THERMAL RESISTANCE OF THE INTERSTITIAL GAS IN THE SMOLUCHOWSKI REGIME:

The integral of the thermal resistance of the interstitial gas in the Knudsen regime (Smoluchowski effect) of the macrogap in the wall region $R_{\lambda,W}$ is derived by the procedure displayed below. The integration parameter displayed in Eq. (5.60) is:

$$2\pi k_g R_{\lambda,W} = \left[\int_{r_a}^{r_{\lambda,W}} \frac{r}{r_p - \omega_0 - \sqrt{r_p^2 - r^2} + j} dr\right]^{-1} \tag{E.19}$$

If $A_{\lambda,W} = r_p + j - \omega_0$, the indefinite integral is given as:

$$\int \frac{r}{a - \sqrt{b^2 - r^2}} dr = a \ln\left|\sqrt{b^2 - r^2} - a\right| + \sqrt{b^2 - r^2} \tag{E.20}$$

Thus:

$$\int_{r_a}^{r_{\lambda,W}} \frac{r}{r_p - \omega_0 - \sqrt{r_p^2 - r^2} + j} dr = \left[A_{\lambda,W} \ln\left|\sqrt{r_p^2 - r^2} - A_{\lambda,W}\right| + \sqrt{r_p^2 - r^2}\right]_{r_a}^{r_{\lambda,W}} \tag{E.21}$$

$$= \left[A_{\lambda,W} \ln\left|\sqrt{r_p^2 - r_{\lambda,W}^2} - A_{\lambda,W}\right| + \sqrt{r_p^2 - r_{\lambda,W}^2}\right] - \left[A_{\lambda,W} \ln\left|\sqrt{r_p^2 - r_a^2} - A_{\lambda,W}\right| + \sqrt{r_p^2 - r_a^2}\right] \tag{E.22}$$

If $B_{\lambda,W} = \sqrt{r_p^2 - r_{\lambda,W}^2}$ and $C_\lambda = \sqrt{r_p^2 - r_a^2}$, then:

$$= \left[A_{\lambda,W} \ln\left|B_{\lambda,W} - A_{\lambda,W}\right| + B_{\lambda,W}\right] - \left[A_{\lambda,W} \ln\left|C_{\lambda,W} - A_{\lambda,W}\right| + C_{\lambda,W}\right] \tag{E.23}$$

$$= \left[A_{\lambda,W} \ln\left|\frac{B_{\lambda,W} - A_{\lambda,W}}{C_{\lambda,W} - A_{\lambda,W}}\right| + B_{\lambda,W} - C_{\lambda,W}\right] \tag{E.24}$$

Thus, substituting Eq. (E.24) into Eq. (E.19) yields:

$$R_{\lambda,W} = \frac{1}{2\pi k_g \left(A_{\lambda,W} \ln\left|\frac{B_{\lambda,W} - A_{\lambda,W}}{C_{\lambda,W} - A_{\lambda,W}}\right| + B_{\lambda,W} - C_{\lambda,W} \right)} \tag{E.25}$$

THERMAL RESISTANCE OF THE INTERSTITIAL GAS IN THE MACRO GAP:

The integral of the thermal resistance in the interstitial gas situated in the macrogap at the wall region $R_{G,W}$ is derived as follows.

The integration parameter displayed in Eq. (5.64) is:

$$R_{G,W} = \frac{1}{2\pi k_g} \left[\int_{r_{\lambda,W}}^{r_p} \frac{r}{r_p - \omega_0 - \sqrt{r_p^2 - r^2}} dr \right]^{-1} \tag{E.26}$$

If $A_G = r_p - \omega_0$, the indefinite integral is given by Eq. (E.20), thus:

$$\int_{r_{\lambda,W}}^{r_p} \frac{r}{r_p - \omega_0 - \sqrt{r_p^2 - r^2}} dr = \left[A_{G,W} \ln\left| \sqrt{r_p^2 - r^2} - A_{G,W} \right| + \sqrt{r_p^2 - r^2} \right]_{r_{\lambda,W}}^{r_p} \tag{E.27}$$

$$= \left[A_{G,W} \ln\left| \sqrt{r_p^2 - r_p^2} - A_{G,W} \right| + \sqrt{r_p^2 - r_p^2} \right] - \left[A_{G,W} \ln\left| \sqrt{r_p^2 - r_{\lambda,W}^2} - A_{G,W} \right| + \sqrt{r_p^2 - r_{\lambda,W}^2} \right] \tag{E.28}$$

If $B_{G,W} = \sqrt{r_p^2 - r_{\lambda,W}^2}$, then:

$$= A_{G,W} \ln\left|A_{G,W}\right| - A_{G,W} \ln\left|B_{G,W} - A_{G,W}\right| - B_{\lambda,W} \tag{E.29}$$

$$= \left[A_{G,W} \ln\left| \frac{A_{G,W}}{B_{G,W} - A_{G,W}} \right| - B_{G,W} \right] \tag{E.30}$$

Thus, substituting Eq. (E.30) into Eq. (E.26) yields:

$$R_{G,W} = \frac{1}{2\pi k_g \left(A_{G,W} \ln\left| \frac{A_{G,W}}{B_{G,W} - A_{G,W}} \right| - B_{G,W} \right)} \tag{E.31}$$

THERMAL RESISTANCE OF THE OUTER SOLID REGION:

The bulk outer solid resistance $R_{out,1,W}$ is derived by the following procedure:

The integration parameter displayed in Eq. (5.31) is rewritten as:

$$\frac{Q_y}{k_s \pi}\int_0^{r_p-2L_{out}} \frac{1}{\left(r_p^2 - r_{\lambda,W}^2 - y^2\right)}\partial y = -\int_{T_2}^{T_1}\partial T \tag{E.32}$$

where $L_{out} = 2\left(\omega_0 + 10\lambda\right)$ with T_1 the temperature in the centre of the pebble and T_2 the temperature at a distance $2L_{out}$ from the origin in the y direction, as displayed in Figure 5.3.

The indefinite integral is given as:

$$\int \frac{1}{a^2 - b^2 - y^2} dy = \frac{\ln\left|y + \sqrt{a-b}\sqrt{b+a}\right| - \ln\left|y - \sqrt{a-b}\sqrt{b+a}\right|}{2\sqrt{a-b}\sqrt{b+a}} \tag{E.33}$$

Thus:

$$\int_0^{r_p-2L_{out}} \frac{1}{r_p^2 - r_{\lambda,W}^2 - y^2} dy = \frac{Q_y}{k_s \pi}\left[\frac{\ln\left|\dfrac{y + \sqrt{r_p^2 - r_{\lambda,W}^2}}{y - \sqrt{r_p^2 - r_{\lambda,W}^2}}\right|}{2\sqrt{r_p^2 - r_{\lambda,W}^2}}\right]_0^{r_p-2L_{out}} \tag{E.34}$$

If $A_{out,W} = r_p - 2L_{out} = r_p - 2\left(\omega_0 + 10\lambda\right)$ and $B_{out,W} = \sqrt{r_p^2 - r_{\lambda,W}^2}$, then the thermal resistance in the outer bulk solid region for one sphere is:

$$R_{out,1,W} = \frac{\ln\left|\dfrac{A_{out,W} + B_{out,W}}{A_{out,W} - B_{out,W}}\right|}{2k_s \pi B_{out,W}} \tag{E.35}$$

where $r_{\lambda,W}$ is the mean free-path radius, defined in Eq. (5.59).

APPENDIX F: DEVELOPMENT OF THE NON-ISOTHERMAL CORRECTION FACTOR

For each emissivity, a data table was constructed. T_{outer} and T_{mid} represent the outer and middle temperature on the flat surface of sphere 2, respectively. Grid independence was also tested in the CFD calculations and it was found that a mesh size of 4 mm would be sufficient. A comparison between the obtained reworked CFD results and the proposed curve-fit correlation displayed in Eq. (5.84) is shown in Figure F.1. The empirical constants' formulas and values are displayed in Figure F.2 and Table F.1. The derivation of the non-isothermal correction factor for the various emissivities is shown in Table F.2 to Table F.6.

Table F.1: Empirical constants for the non-isothermal correction factor

VARIABLE	$\varepsilon_r = 1.0$	$\varepsilon_r = 0.8$	$\varepsilon_r = 0.6$	$\varepsilon_r = 0.4$	$\varepsilon_r = 0.2$
a_1	-0.40328	-0.35243	-0.32617	-0.29790	-0.22449
a_2	0.74933	0.62742	0.50588	0.38431	0.26152
a_3	0.58119	0.63771	0.65059	0.67257	0.94184
a_4	1.04946	1.02342	1.01016	1.00198	0.99678

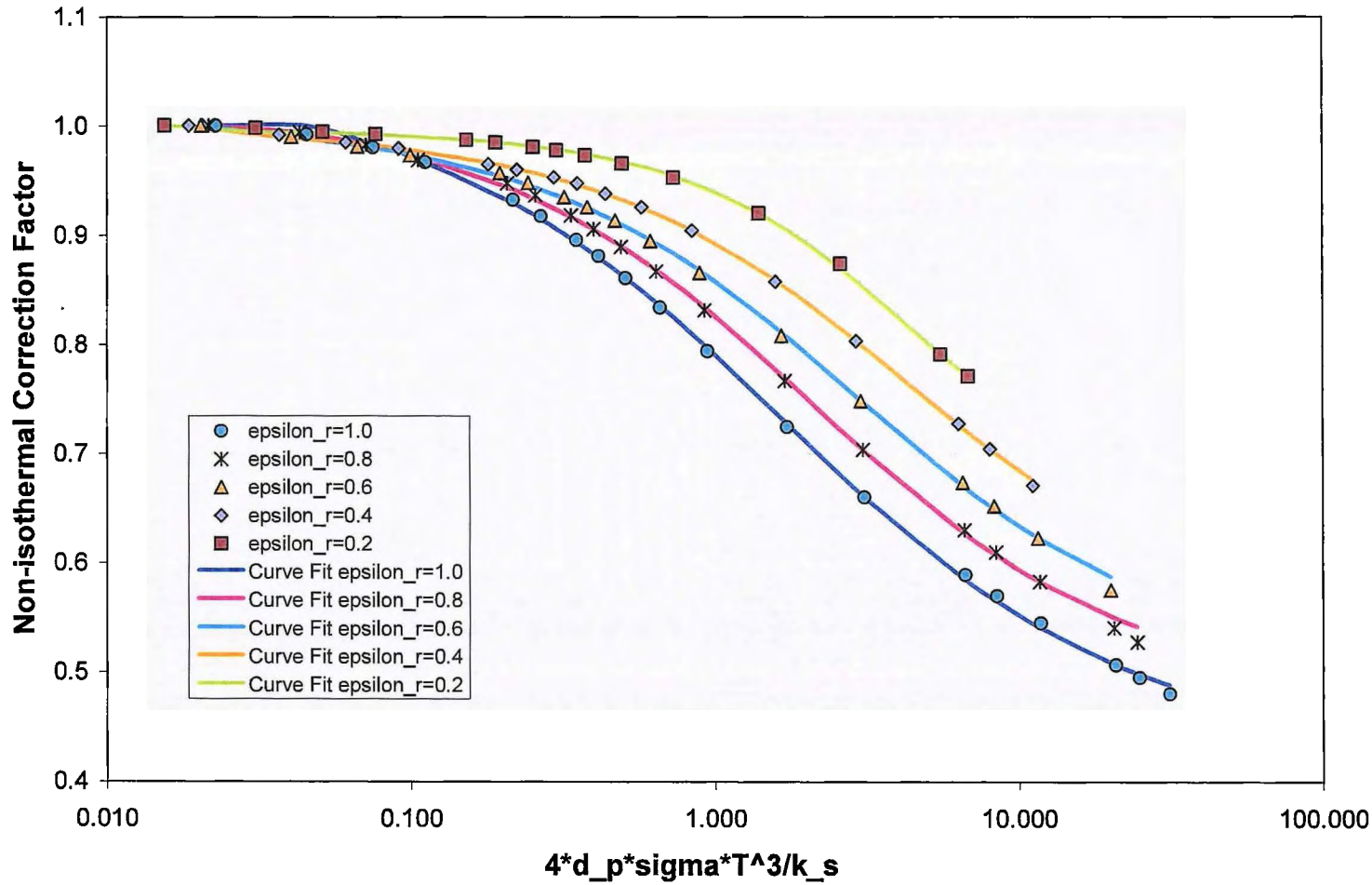

Figure F.1: Comparison between proposed correlation and Computational Fluid Dynamics results

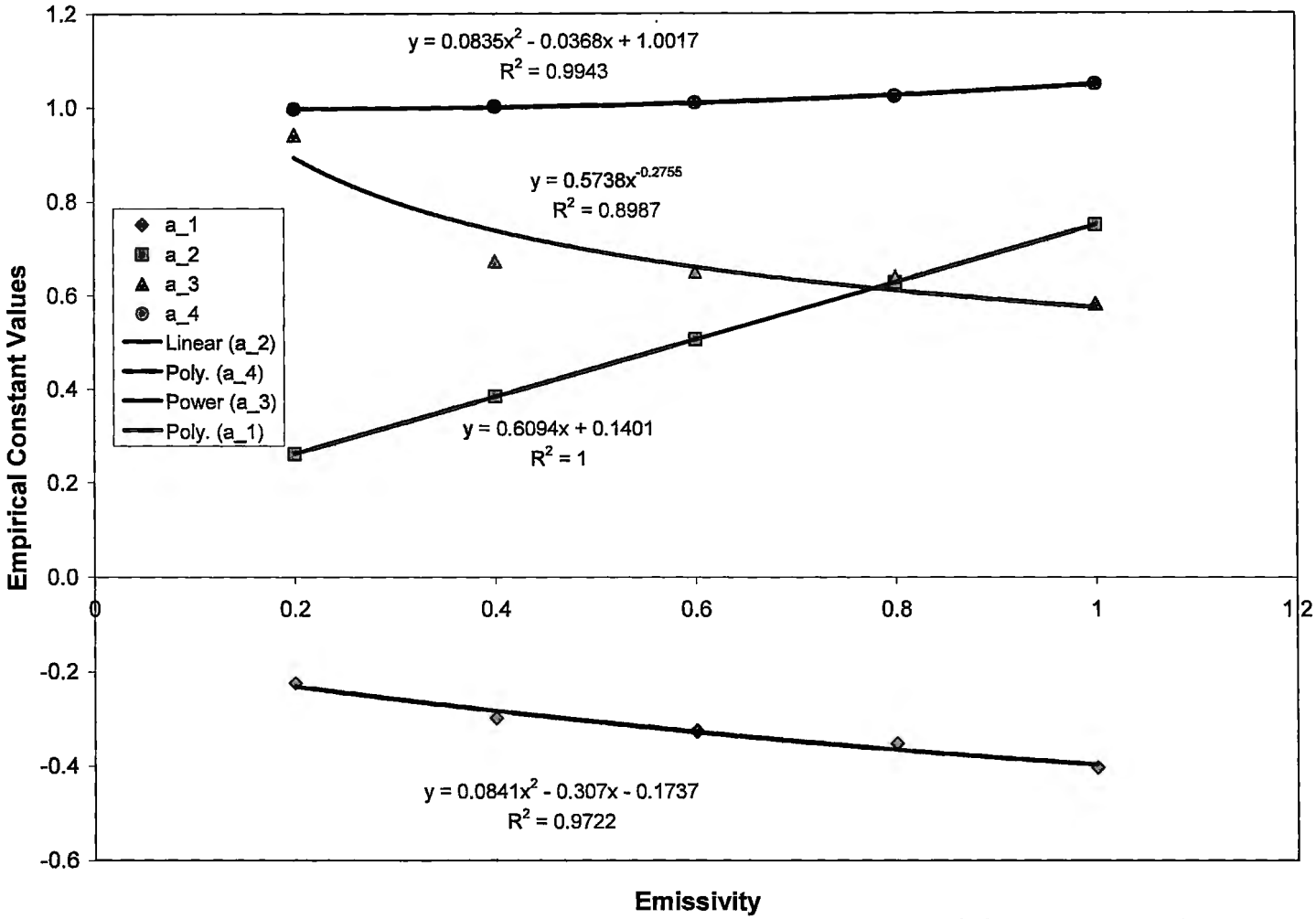

Figure F.2: Comparison between proposed correlation and Computational Fluid Dynamics results

Table F.2: Derivation to calculate the non-isothermal correction factor for $\varepsilon_r = 1.0$

$\varepsilon_r = 1.0$		SPHERE 1	SPHERE 2	SPHERE 2						$f_k = \frac{k_r}{k_{r,max}}$
k_s	$1/k_s$	T_1 [°C]	T_{outer} [°C]	T_{mid} [°C]	$T_{avg,S2} = \frac{(T_{outer} + T_{mid})}{2}$	$T_{avg,2} = \frac{(T_1 + T_{avg,S2})}{2}$	$\frac{4d_p\sigma(T_{avg,2} + 273.15)^3}{k_s}$	Q_{in} [W/m^2]	$k_r = \frac{Q_{in}d_p}{(T_1 - T_{avg,S2})}$	Normalised
1000.0	0.001	1200	630.920	631.580	631.250	915.625	0.023	1000.000	0.10549	1.000
500.0	0.002	1200	625.880	627.180	626.530	913.265	0.045		0.10463	0.992
300.0	0.003	1200	618.600	620.690	619.645	909.823	0.075		0.10338	0.980
200.0	0.005	1200	610.110	613.130	611.620	905.810	0.112		0.10197	0.967
100.0	0.010	1200	587.150	592.570	589.860	894.930	0.217		0.09834	0.932
80.0	0.013	1200	576.660	583.110	579.885	889.943	0.268		0.09676	0.917
60.0	0.017	1200	560.750	568.720	564.735	882.368	0.350		0.09445	0.895
50.0	0.020	1200	549.750	558.800	554.275	877.138	0.414		0.09292	0.881
40.0	0.025	1200	534.000	544.450	539.225	869.613	0.508		0.09080	0.861
30.0	0.033	1200	511.720	524.150	517.935	858.968	0.658		0.08797	0.834
20.0	0.050	1200	475.850	491.240	483.545	841.773	0.943		0.08375	0.794
10.0	0.100	1200	404.890	425.330	415.110	807.555	1.718		0.07644	0.725
5.0	0.200	1200	326.610	351.210	338.910	769.455	3.085		0.06968	0.661
2.0	0.500	1200	221.240	248.480	234.860	717.430	6.614		0.06217	0.589
1.5	0.667	1200	188.840	215.950	202.395	701.198	8.392		0.06014	0.570
1.0	1.000	1200	143.880	169.730	156.805	678.403	11.725		0.05752	0.545
0.5	2.000	1200	68.321	88.078	78.200	639.100	20.663		0.05349	0.507
0.4	2.500	1200	43.725	60.143	51.934	625.967	24.729		0.05226	0.495
0.3	3.333	1200	11.192	21.908	16.550	608.275	31.064		0.05070	0.481

Table F.3: Derivation to calculate the non-isothermal correction factor for $\varepsilon_r = 0.8$

$\varepsilon_r = 0.8$		SPHERE 1	SPHERE 2	SPHERE 2						$f_k = \frac{k_r}{k_{r,max}}$
k_s	$1/k_s$	T_1 [°C]	T_{outer} [°C]	T_{mid} [°C]	$T_{avg,S2} = \frac{(T_{outer} + T_{mid})}{2}$	$T_{avg,2} = \frac{(T_1 + T_{avg,S2})}{2}$	$\frac{4 d_p \sigma (T_{avg,2} + 273.15)^3}{k_s}$	Q_{in} [W/m^2]	$k_r = \frac{Q_{in} d_p}{(T_1 - T_{avg,S2})}$	Normalised
1000.0	0.001	1200	589.230	589.670	589.450	894.725	0.022	1000.000	0.098	1.000
500.0	0.002	1200	585.230	586.090	585.660	892.830	0.043		0.098	0.994
300.0	0.003	1200	577.670	579.070	578.370	889.185	0.071		0.097	0.982
200.0	0.005	1200	568.630	570.640	569.635	884.818	0.106		0.095	0.969
100.0	0.010	1200	553.670	557.390	555.530	877.765	0.207		0.093	0.947
80.0	0.013	1200	545.520	549.990	547.755	873.878	0.257		0.092	0.936
60.0	0.017	1200	532.040	537.600	534.820	867.410	0.337		0.090	0.918
50.0	0.020	1200	522.440	528.810	525.625	862.813	0.399		0.089	0.905
40.0	0.025	1200	509.600	517.050	513.325	856.663	0.491		0.087	0.889
30.0	0.033	1200	490.990	499.980	495.485	847.743	0.639		0.085	0.867
20.0	0.050	1200	459.730	471.100	465.415	832.708	0.920		0.082	0.831
10.0	0.100	1200	395.850	411.500	403.675	801.838	1.691		0.075	0.767
5.0	0.200	1200	322.630	342.060	332.345	766.173	3.056		0.069	0.704
2.0	0.500	1200	220.250	242.420	231.335	715.668	6.579		0.062	0.630
1.5	0.667	1200	187.850	210.040	198.945	699.473	8.348		0.060	0.610
1.0	1.000	1200	142.280	163.540	152.910	676.455	11.653		0.057	0.583
0.5	2.000	1200	63.188	79.382	71.285	635.643	20.429		0.053	0.541
0.4	2.500	1200	36.581	49.924	43.253	621.626	24.373		0.052	0.528

Table F.4: Derivation to calculate the non-isothermal correction factor for $\varepsilon_r = 0.6$

$\varepsilon_r = 0.6$		SPHERE 1	SPHERE 2	SPHERE 2						$f_k = \frac{k_r}{k_{r,max}}$
k_s	$1/k_s$	T_1 [°C]	T_{outer} [°C]	T_{mid} [°C]	$T_{avg,S2} = \frac{(T_{outer} + T_{mid})}{2}$	$T_{avg,2} = \frac{(T_1 + T_{avg,S2})}{2}$	$\frac{4 d_p \sigma (T_{avg,2} + 273.15)^3}{k_s}$	Q_{in} [W/m^2]	$k_r = \frac{Q_{in} d_p}{(T_1 - T_{avg,S2})}$	Normalised
1000.0	0.001	1200	542.000	542.270	542.135	871.068	0.020	1000.000	0.091	1.000
500.0	0.002	1200	535.050	535.560	535.305	867.653	0.040		0.090	0.990
300.0	0.003	1200	528.570	529.410	528.990	864.495	0.067		0.089	0.980
200.0	0.005	1200	523.100	524.320	523.710	861.855	0.099		0.089	0.973
100.0	0.010	1200	511.000	513.280	512.140	856.070	0.196		0.087	0.956
80.0	0.013	1200	504.270	507.020	505.645	852.823	0.243		0.086	0.947
60.0	0.017	1200	494.120	497.600	495.860	847.930	0.320		0.085	0.934
50.0	0.020	1200	487.040	491.060	489.050	844.525	0.380		0.084	0.925
40.0	0.025	1200	477.120	481.880	479.500	839.750	0.469		0.083	0.913
30.0	0.033	1200	461.430	467.260	464.345	832.173	0.613		0.082	0.894
20.0	0.050	1200	435.850	443.420	439.635	819.818	0.888		0.079	0.865
10.0	0.100	1200	380.520	391.400	385.960	792.980	1.649		0.074	0.808
5.0	0.200	1200	313.700	327.730	320.715	760.358	3.005		0.068	0.748
2.0	0.500	1200	215.170	231.740	223.455	711.728	6.500		0.061	0.674
1.5	0.667	1200	182.790	199.460	191.125	695.563	8.247		0.059	0.652
1.0	1.000	1200	135.990	152.000	143.995	671.998	11.490		0.057	0.623
0.5	2.000	1200	50.560	62.530	56.545	628.273	19.936		0.052	0.575

Table F.5: Derivation to calculate the non-isothermal correction factor for $\varepsilon_r = 0.4$

$\varepsilon_r = 0.4$		SPHERE 1	SPHERE 2	SPHERE 2						$f_k = \frac{k_r}{k_{r,max}}$
k_s	$1/k_s$	T_1 [°C]	T_{outer} [°C]	T_{mid} [°C]	$T_{avg,S2} = \frac{(T_{outer} + T_{mid})}{2}$	$T_{avg,2} = \frac{(T_1 + T_{avg,S2})}{2}$	$\frac{4 d_p \sigma (T_{avg,2} + 273.15)^3}{k_s}$	Q_{in} [W/m^2]	$k_r = \frac{Q_{in} d_p}{(T_1 - T_{avg,S2})}$	Normalised
1000.0	0.001	1200	474.700	474.830	474.765	837.383	0.019	1000.000	0.083	1.000
500.0	0.002	1200	468.490	468.730	468.610	834.305	0.037		0.082	0.992
300.0	0.003	1200	463.160	463.560	463.360	831.680	0.061		0.081	0.985
200.0	0.005	1200	458.880	459.470	459.175	829.588	0.091		0.081	0.979
100.0	0.010	1200	447.560	448.670	448.115	824.058	0.180		0.080	0.965
80.0	0.013	1200	443.580	444.940	444.260	822.130	0.224		0.079	0.960
60.0	0.017	1200	437.860	439.600	438.730	819.365	0.296		0.079	0.953
50.0	0.020	1200	433.280	435.330	434.305	817.153	0.353		0.078	0.947
40.0	0.025	1200	425.180	427.630	426.405	813.203	0.436		0.078	0.937
30.0	0.033	1200	414.600	417.660	416.130	808.065	0.573		0.077	0.925
20.0	0.050	1200	395.690	399.800	397.745	798.873	0.838		0.075	0.904
10.0	0.100	1200	351.100	357.340	354.220	777.110	1.577		0.071	0.857
5.0	0.200	1200	292.810	301.250	297.030	748.515	2.903		0.066	0.803
2.0	0.500	1200	198.220	208.550	203.385	701.693	6.304		0.060	0.728
1.5	0.667	1200	165.140	175.570	170.355	685.178	7.985		0.058	0.704
1.0	1.000	1200	114.570	124.460	119.515	659.758	11.049		0.056	0.671

Table F.6: Derivation to calculate the non-isothermal correction factor for $\varepsilon_r = 0.2$

$\varepsilon_r = 0.2$		SPHERE 1	SPHERE 2	SPHERE 2						$f_k = \frac{k_r}{k_{r,max}}$
k_s	$1/k_s$	T_1 [°C]	T_{outer} [°C]	T_{mid} [°C]	$T_{avg,S2} = \frac{(T_{outer} + T_{mid})}{2}$	$T_{avg,2} = \frac{(T_1 + T_{avg,S2})}{2}$	$\frac{4 d_p \sigma (T_{avg,2} + 273.15)^3}{k_s}$	Q_{in} [W/m^2]	$k_r = \frac{Q_{in} d_p}{(T_1 - T_{avg,S2})}$	Normalised
1000.0	0.001	1200	342.920	342.950	342.935	771.468	0.016	1000.000	0.070	1.000
500.0	0.002	1200	341.100	341.170	341.135	770.568	0.031		0.070	0.998
300.0	0.003	1200	337.760	337.870	337.815	768.908	0.051		0.070	0.994
200.0	0.005	1200	335.950	336.100	336.025	768.013	0.077		0.069	0.992
100.0	0.010	1200	331.310	331.620	331.465	765.733	0.153		0.069	0.987
80.0	0.013	1200	329.150	329.520	329.335	764.668	0.190		0.069	0.984
60.0	0.017	1200	325.400	325.880	325.640	762.820	0.252		0.069	0.980
50.0	0.020	1200	322.690	323.270	322.980	761.490	0.301		0.068	0.977
40.0	0.025	1200	318.410	319.110	318.760	759.380	0.375		0.068	0.973
30.0	0.033	1200	311.520	312.410	311.965	755.983	0.494		0.068	0.965
20.0	0.050	1200	299.180	300.410	299.795	749.898	0.729		0.067	0.952
10.0	0.100	1200	267.250	269.250	268.250	734.125	1.391		0.064	0.920
5.0	0.200	1200	217.540	220.410	218.975	709.488	2.582		0.061	0.874
2.0	0.500	1200	114.450	117.980	116.215	658.108	5.495		0.055	0.791
1.5	0.667	1200	65.756	69.173	67.465	633.732	6.767		0.053	0.771

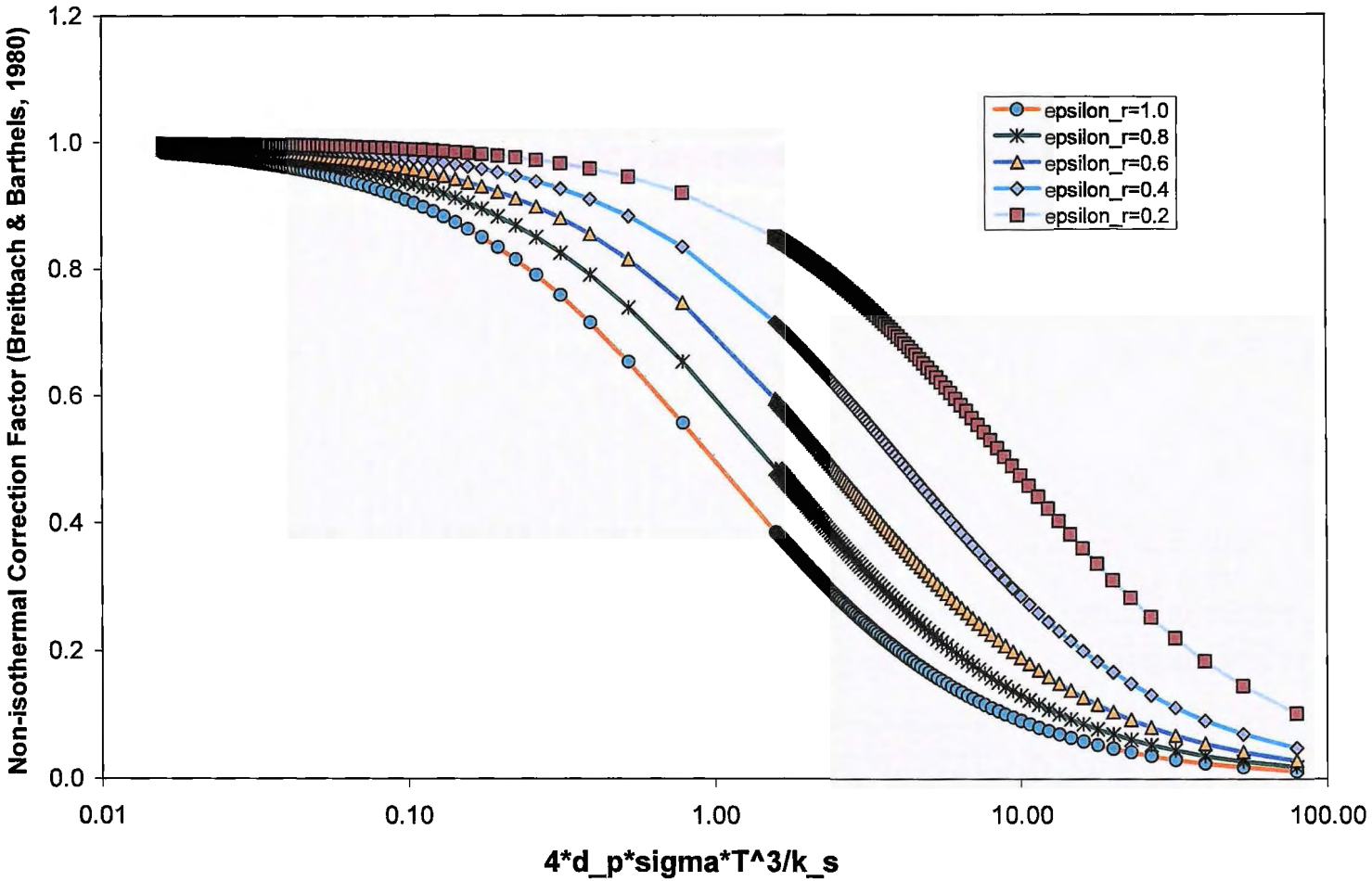

Figure F.3: Non-isothermal correction factor (Breitbach & Barthels, 1980:392)

APPENDIX G: COMPUTER CODES

G.1 COORDINATION AND CONTACT-ANGLE CALCULATION CODE

This section presents the code for calculating the coordination number and the average contact angle for the given coordinates of a numerical packed bed.

```
// CONumber.cpp : Defines the entry point for the console
application.
//

#include "stdafx.h"
#include "math.h"

const int MAXSIZE =20635;
const int BALL = 12;
int _tmain(int argc, _TCHAR* argv[])
{
      FILE *hFile;
      hFile = fopen("D:\\University\\PhD
Studies\\Werner\\CONumber\\CONumber\\Debug\\coord.txt","r");
      double *x = new double[MAXSIZE];
      double *y = new double[MAXSIZE];
      double *z = new double[MAXSIZE];
      double **dist = new double*[MAXSIZE];
      for (int i=0; i<=MAXSIZE;i++)
      {
            dist[i] = new double[12];
      }

      int **bnr = new int*[MAXSIZE];
      for (int i=0; i<=MAXSIZE;i++)
      {
            bnr[i] = new int[12];
      }
      double Co_dist=60.002;
      double pi=3.141592654;
      int p;
      double distance;
      double r1;
      double r2;
      double difference;
      double theta;
      double heat_flow_angle;
      double Co_num;
      double con1=1;
      double con2=0;
      int sum=MAXSIZE+1;

      for (int i =0 ; i<=MAXSIZE;i++)
      {
            fscanf( hFile, "%lf", (x+i) );
            fscanf( hFile, "%lf", (y+i) );
            fscanf( hFile, "%lf", (z+i) );
```

```
        }

        FILE *outFile;
        outFile = fopen("output.txt","w");
        FILE *outFile2;
        outFile2 = fopen("output2.txt","w");
        int l =0;

        for(int j=0;j<MAXSIZE;j++)
        {
              for(int k=0;k<MAXSIZE;k++)
              {
                    distance=sqrt(pow((x[j]-x[k]),2)+pow((y[j]-
y[k]),2)+pow((z[j]-z[k]),2));

                    if (distance <= Co_dist)
                    {
                          dist[j][l]=distance;
                          bnr[j][l]=k;

                          r1=sqrt(pow(x[j],2)+pow(y[j],2));
                          r2=sqrt(pow(x[k],2)+pow(y[k],2)+pow((z[j]-
z[k]),2));
                          theta=asin((pow(r2,2)-pow(r1,2)-
pow(distance,2))/(-2*r1*distance)); //Law of cosine
                          theta=theta*180/pi;
                          theta=abs(theta);   //To calculate average
contact angle
                          //fprintf(outFile,"%i %lf
",bnr[j][l],dist[j][l]);
                          if (theta>0)
                          {
                                fprintf(outFile,"%i %lf
",bnr[j][l],theta);     //Print Ball number and contact angle out to
output1.txt
                          }

                    l++;

                    }

              }
                    Co_num=l-1;  //Subtrackting 1
                    fprintf(outFile2,"%i %lf ",j,Co_num);
                    fprintf(outFile2,"\n");

                    l=0;
                    fprintf(outFile,"\n");

        }
        fclose(hFile);
        fclose(outFile);
        fclose(outFile2);

        return 0;
}
```

G.2 MULTI-SPHERE UNIT CELL CALCULATION CODE

Analysis of the effective thermal conductivity against the various experimental data sets was conducted by programming the Multi-sphere Unit Cell in Engineering Equation Solver (EES). The same flowchart as presented in Figure 7.1 was used to program the Multi-sphere Unit Cell Model. This section presents the EES code used to simulate the HTTU experimental test facility.

PROCEDURE MacroContact(r_eq,F_bah,E_young_1,E_young_2,mu_1,mu_2,k_1,k_2:R_L,a_H)

$$a_H := \left[\frac{0.75 \cdot F_{bah} \cdot r_{eq} \cdot (1 - \mu_1^{\,2})}{E_{young,1}}\right]^{(1/3)}$$

$$R_L := \frac{0.64}{k_1 \cdot a_H}$$

End MacroContact

PROCEDURE InnerBulk(a_H,k_s,d_p,omega_0:R_B_in1_2)

$$R_{B,in1,2} := \frac{d_p - \omega_0}{k_s \cdot \pi \cdot a_H^{\,2}}$$

End InnerBulk

PROCEDURE MidBulk(a_H,r_eq,k_s,d_p,omega_0,radius_lambda:R_B_mid1_2)

$$R_{B,mid1,2} := \frac{d_p - \omega_0}{k_s \cdot \pi \cdot (radius_{lambda}^{\,2} - a_H^{\,2})}$$

End MidBulk

PROCEDURE LambdaGas(k_f,omega_0,j_gas,r_p,radius_lambda,a_H:R_lambda)

$$AA := 2 \cdot r_p + j_{gas} - \omega_0$$

$$BB := \sqrt{r_p^{\,2} - radius_{lambda}^{\,2}}$$

$$CC := \sqrt{r_p^{\,2} - a_H^{\,2}}$$

$$R_{lambda} := \frac{2}{\pi \cdot k_f \cdot \left[AA \cdot \ln\left(\left|\frac{AA - 2 \cdot BB}{AA - 2 \cdot CC}\right|\right) + 2 \cdot BB - 2 \cdot CC\right]}$$

End LambdaGas

PROCEDURE BulkGas(r_p,omega_0,radius_lambda,k_f:R_G)

$$A_G := 2 \cdot r_p - \omega_0$$

$$B_G := \sqrt{r_p^{\,2} - radius_{lambda}^{\,2}}$$

$$R_G := \frac{2}{\pi \cdot k_f \cdot \left[A_G \cdot \ln\left(\left|\frac{A_G}{A_G - 2 \cdot B_G}\right|\right) - 2 \cdot B_G\right]}$$

End BulkGas

PROCEDURE OuterBulk(r_p,omega_0,radius_lambda,lambda_meanfree,k_s:R_B_out1_2,A_out,B_out)

$$A_{out} := r_p - 2 \cdot (0.5 \cdot \omega_0 + 5 \cdot \lambda_{meanfree})$$

$$B_{out} := \sqrt{r_p^{\,2} - radius_{lambda}^{\,2}}$$

$$R_{B,out1,2} := \frac{\ln\left[\left|\frac{A_{out} + B_{out}}{A_{out} - B_{out}}\right|\right]}{k_s \cdot \pi \cdot B_{out}}$$

End OuterBulk

PROCEDURE InnerBulkWall(a_H,k_s,d_p,omega_0:R_B_in1_2)

$$R_{B,in1,2} := \frac{d_p - \omega_0}{2 \cdot k_s \cdot \pi \cdot a_H^{\,2}}$$

End InnerBulkWall

PROCEDURE MidBulkWall(a_H,r_eq,k_s,d_p,omega_0,radius_lambda:R_B_mid1_2)

$$R_{B,mid1,2} := \frac{d_p - \omega_0}{2 \cdot k_s \cdot \pi \cdot (radius_{lambda} - a_H)^2}$$

End MidBulkWall

PROCEDURE LambdaGasWall(k_f,omega_0,j_gas,r_p,radius_lambda,a_H:R_lambda)

$$AA := r_p + j_{gas} - \omega_0$$

$$BB := \sqrt{r_p^2 - radius_{lambda}^2}$$

$$CC := \sqrt{r_p^2 - a_H^2}$$

$$R_{lambda} := \frac{1}{2 \cdot \pi \cdot k_f \cdot \left[AA \cdot \ln\left(\left| \frac{BB - AA}{CC - AA} \right| \right) + BB - CC \right]}$$

End LambdaGasWall

PROCEDURE BulkGasWall(r_p,omega_0,radius_lambda,k_f:R_G)

$$A_G := r_p - \omega_0$$

$$B_G := \sqrt{r_p^2 - radius_{lambda}^2}$$

$$R_G := \frac{1}{2 \cdot \pi \cdot k_f \cdot \left[A_G \cdot \ln\left(\left| \frac{A_G}{B_G - A_G} \right| \right) - B_G \right]}$$

End BulkGasWall

PROCEDURE OuterBulkWall(r_p,omega_0,radius_lambda,lambda_meanfree,k_s:R_B_out1_2,A_out,B_out)

$$A_{out} := r_p - 2 \cdot (\omega_0 + 10 \cdot \lambda_{meanfree})$$

$$B_{out} := \sqrt{r_p^2 - radius_{lambda}^2}$$

$$R_{B,out1,2} := \frac{\ln\left[\left| \frac{A_{out} + B_{out}}{A_{out} - B_{out}} \right| \right]}{2 \cdot k_s \cdot \pi \cdot B_{out}}$$

End OuterBulkWall

PROCEDURE RadiationShortBulk(N_c,d_p,sigma_r,T_K,epsilon_r,F_12,f_k,phi_rad:k_e_r_S)

$$A_s := 4 \cdot \pi \cdot \left[\frac{d_p}{2} \right]^2$$

$$A_r := d_p^2$$

$$k_{e,r,S} := \frac{2 \cdot N_c \cdot d_p \cdot \sigma_r \cdot A_s \cdot T_K^3}{A_r \cdot \left[\frac{2 - 2 \cdot \varepsilon_r}{\varepsilon_r} + \frac{1}{F_{12}} \right]} \cdot f_k \cdot \sin(\phi_{rad})$$

End RadiationShortBulk

PROCEDURE RadiationLongBulk(d_p,sigma_r,T_K,epsilon_r,F_12,f_k:k_e_r_L)

$$A_s := 4 \cdot \pi \cdot \left[\frac{d_p}{2} \right]^2$$

$$A_r := d_p^2$$

$$k_{e,r,L} := \frac{4.7 \cdot 5.32 \cdot d_p \cdot \sigma_r \cdot A_s \cdot T_K^3}{A_r \cdot \left[\frac{2 - 2 \cdot \varepsilon_r}{\varepsilon_r} + \frac{1}{F_{12}} \right]} \cdot f_k$$

End RadiationLongBulk

PROCEDURE RadiationShortWall(d_p,sigma_r,T_K,epsilon_r_1,epsilon_r_2,f_k,SW_WS,F_12_wall_short,F_21_wall_short:k_e_r_S_W)

$$A_1 := 4 \cdot \pi \cdot \left[\frac{d_p}{2} \right]^2$$

$$A_2 := 63.68 \cdot \pi \cdot \left[\frac{d_p}{2} \right]^2$$

$A_r := d_p^2$

If (SW_{WS} = 1) Then

$$k_{e,r,S,W} := \frac{2 \cdot d_p \cdot \sigma_r \cdot T_K^3}{A_r \cdot \left[\frac{1 - \varepsilon_{r,1}}{\varepsilon_{r,1} \cdot A_1} + \frac{1}{A_1 \cdot F_{12,wall,short}} + \frac{1 - \varepsilon_{r,2}}{\varepsilon_{r,2} \cdot A_2}\right]} \cdot f_k$$

$$k_{e,r,S,W} := \frac{2 \cdot d_p \cdot \sigma_r \cdot T_K^3}{A_r \cdot \left[\frac{1 - \varepsilon_{r,2}}{\varepsilon_{r,2} \cdot A_2} + \frac{1}{A_2 \cdot F_{21,wall,short}} + \frac{1 - \varepsilon_{r,1}}{\varepsilon_{r,1} \cdot A_1}\right]} \cdot f_k$$

End RadiationShortWall

PROCEDURE RadiationLongWall(d_p,sigma_r,T_K,epsilon_r_1,epsilon_r_2,F_12_wall_eff,f_k:k_e_r_L_W)

$$A_1 := 4 \cdot \pi \cdot \left[\frac{d_p}{2}\right]^2$$

$$A_2 := 63.68 \cdot \pi \cdot \left[\frac{d_p}{2}\right]^2$$

$A_r := d_p^2$

$$k_{e,r,L,W} := \frac{4.536 \cdot d_p \cdot \sigma_r \cdot T_K^3}{A_r \cdot \left[\frac{1 - \varepsilon_{r,1}}{\varepsilon_{r,1} \cdot A_1} + \frac{1}{A_1 \cdot F_{12,wall,eff}} + \frac{1 - \varepsilon_{r,2}}{\varepsilon_{r,2} \cdot A_2}\right]} \cdot f_k$$

End RadiationLongWall

PROCEDURE Contact_Kavainy(epsilon,d_p:S,S_F,N_A1,N_L1)

$$R := \frac{d_p}{2}$$

If (ε >= 0.35) Then

$S := 1$

$S_F := 1$

$$N_{A1} := \frac{1}{4 \cdot R^2}$$

$$N_{L1} := \frac{1}{2 \cdot R}$$

If ((ε < 0.35) and (ε >= 0.2595)) Then

$S := 0.25$

$$S_F := \frac{\sqrt{3}}{4}$$

$$N_{A1} := \frac{3}{16 \cdot R^2}$$

$$N_{L1} := \frac{\sqrt{3}}{2 \cdot R}$$

$S := 1 / 3$

$$S_F := \frac{1}{\sqrt{6}}$$

$$N_{A1} := \frac{1}{2 \cdot \sqrt{3} \cdot R^2}$$

$$N_{L1} := \frac{\sqrt{3 / 8}}{R}$$

End Contact_Kavainy

If $\left[(r >= R_{in}) \text{ and } \left(r <= \frac{R_{out} + R_{in}}{2}\right)\right]$ Then

$$z_{ball} := \frac{r - R_{in}}{d_p}$$

$$z_{ball} := \frac{R_{out} - r}{d_p}$$

$$\varepsilon := -0.0127 \cdot z_{ball}^{\,2} + 0.0967 \cdot z_{ball} + 0.2011$$

End PorosityCorrection

$$k_{s,star,sphere} = 60$$

$$k_{s,star,S,P} = \frac{2 \cdot k_{s,star,sphere} \cdot k_{s,plate}}{k_{s,star,sphere} + k_{s,plate}}$$

$$k_f = \mathbf{k}('N2', T=T_K)$$

$$k_{s,sphere} = 147.096 - 0.229541 \cdot T_C + 0.000206027 \cdot T_C^{\,2} - 7.1529 \times 10^{-8} \cdot T_C^{\,3}$$

$$T_K = T_C + 273.15$$

$$k_{s,plate} = 147.096 - 0.229541 \cdot T_C + 0.000206027 \cdot T_C^{\,2} - 7.1529 \times 10^{-8} \cdot T_C^{\,3}$$

$$F_{bah} = 72.307 \cdot Bed_{Depth} + 7.8716$$

$$Bed_{Depth} = 1.2 - Bed_{Height}$$

$$Bed_{Height} = 0.6$$

$$E_{young,sphere} = 7.4 \times 10^{9}$$

$$E_{young,plate} = 7.4 \times 10^{9}$$

$$\mu_{sphere} = 0.3$$

$$\mu_{plate} = 0.3$$

$$Pr = \mathbf{Pr}('N2', T=T_K)$$

$$\gamma_h = \frac{cp}{cv}$$

$$cp = \mathbf{Cp}('N2', T=T_K)$$

$$cv = \mathbf{Cv}('N2', T=T_K)$$

$$\lambda_{meanfree,0} = 0.7387 \cdot 10^{-7}$$

$$\lambda_{meanfree} = \frac{P_0 \cdot T_g}{P_g \cdot T_0} \cdot \lambda_{meanfree,0}$$

$$P_0 = 85000$$

$$P_g = 10000$$

$$T_0 = 20 + 273.15$$

$$T_g = T_K$$

$$M_{gg} = \mathbf{MolarMass}('Nitrogen')$$

$$M_{ss} = 12$$

$$\mu_{vis} = \frac{M_{gg}}{M_{ss}}$$

$$M_{star} = 1.4 \cdot M_{gg}$$

$$T_{00} = 273.15$$

$$\alpha_{T1} = \mathbf{exp}\left[-0.57 \cdot \left(\frac{T_K - T_{00}}{T_{00}}\right)\right] \cdot \left[\frac{M_{star}}{6.8 + M_{star}}\right] + \frac{2.4 \cdot \mu_{vis}}{(1 + \mu_{vis})^2} \cdot \left[1 - \mathbf{exp}\left(-0.57 \cdot \left[\frac{T_K - T_{00}}{T_{00}}\right]\right)\right]$$

$$\alpha_{T2} = \alpha_{T1}$$

$$j_{gas} = \left[\left(\frac{2 - \alpha_{T1}}{\alpha_{T1}} + \frac{2 - \alpha_{T2}}{\alpha_{T2}}\right) \cdot \left(\frac{2 \cdot \gamma_h}{1 + \gamma_h}\right)\right] \cdot \frac{1}{Pr} \cdot \lambda_{meanfree}$$

$$d_p = 0.06$$

$$r_p = \frac{d_p}{2}$$

$$R_{in} = 0.3$$

$$R_{out} = 1.15$$

$$r_{eq,bulk} = r_p$$

$$r_{eq,wall} = r_p$$

$$\omega_{0,bulk} = \frac{a_H^{\,2}}{2 \cdot r_{eq,bulk}}$$

$$\omega_{0,wall} = \frac{a_{H,W}^{\,2}}{2 \cdot r_{eq,wall}}$$

$$radius_{\lambda,bulk} = \sqrt{r_p^{\,2} - (r_p - 0.5 \cdot \omega_{0,bulk} - 5 \cdot \lambda_{meanfree})^2}$$

$$radius_{\lambda,wall} = \sqrt{r_p^{\,2} - (r_p - \omega_{0,wall} - 10 \cdot \lambda_{meanfree})^2}$$

$$\varepsilon_{star} = \frac{\varepsilon_{r,1} + \varepsilon_{r,2}}{2}$$

$$f_k = a_{11} \cdot \arctan\left[a_{22} \cdot \left(\frac{1}{\Lambda}\right)^{a_{33}}\right] + a_{44}$$

$$a_{11} = 0.0841 \cdot \varepsilon_{star}^{\,2} - 0.307 \cdot \varepsilon_{star} - 0.1737$$

$$a_{22} = 0.6094 \cdot \varepsilon_{star} + 0.1401$$

$$a_{33} = 0.5738 \cdot \varepsilon_{star}^{\,-0.2755}$$

$$a_{44} = 0.0835 \cdot \varepsilon_{star}^{\,2} - 0.0368 \cdot \varepsilon_{star} + 1.0017$$

$$\Lambda_{in} = \frac{1}{\Lambda}$$

$$\varepsilon_{r,1} = 0.8$$

$$\varepsilon_{r,2} = 0.8$$

$$\sigma_r = 5.670E{-}08$$

$$F_{12,bulk} = 0.0756$$

$$F_{12,bulk,eff} = 0.0199$$

$$F_{12,wall,Short} = 0.315$$

$$F_{21,wall,Short} = 0.01976$$

$$F_{12,wall,eff} = 0.02356$$

Call PorosityCorrection ($Radius_{radial}$, R_{in} , R_{out} , d_p : f_k , z_{ball})

$$\varepsilon = \mathbf{If}\ (z_{ball} , 3.8 , \varepsilon_{correction} , 0.385 , 0.385)$$

$$N_c = 25.952 \cdot \varepsilon^{\,3} - 62.364 \cdot \varepsilon^{\,2} + 39.724 \cdot \varepsilon - 2.0233$$

$$\phi_c = -6.1248 \cdot N_c^{\,2} + 73.419 \cdot N_c - 186.68$$

$$\phi_{c,rad} = \phi_c \cdot \frac{\pi}{180}$$

Call MacroContact ($r_{eq,bulk}$, F_{bah} , $E_{young,sphere}$, $E_{young,sphere}$, μ_{sphere} , μ_{sphere} , $k_{s,sphere}$, $k_{s,sphere}$: f_k , a_H)

Call InnerBulk (a_H , $k_{s,sphere}$, d_p , $\omega_{0,bulk}$: $R_{B,in1,2}$)

Call MidBulk (a_H , $r_{eq,bulk}$, $k_{s,sphere}$, d_p , $\omega_{0,bulk}$, $radius_{\lambda,bulk}$: $R_{B,mid1,2}$)

Call LambdaGas (k_f , $\omega_{0,bulk}$, j_{gas} , r_p , $radius_{\lambda,bulk}$, a_H : R_{lambda})

Call BulkGas (r_p , $\omega_{0,bulk}$, $radius_{\lambda,bulk}$, k_f : R_G)

Call OuterBulk (r_p , $\omega_{0,bulk}$, $radius_{\lambda,bulk}$, $\lambda_{meanfree}$, $k_{s,sphere}$: R_G , a_H , B_{out})

$$R_T = \left[\frac{1}{R_{B,in1,2}} + \frac{1}{R_{B,mid1,2}} + \frac{1}{R_{B,out1,2}}\right]^{-1}$$

$$R_{m,comb} = \left[\frac{1}{R_L} + \frac{1}{R_\lambda} + \frac{1}{R_G}\right]^{-1}$$

$$R_j = R_T + R_{m,comb}$$

Call MacroContact ($r_{eq,wall}$, F_{bah} , $E_{young,sphere}$, $E_{young,plate}$, μ_{sphere} , μ_{plate} , $k_{s,star,S,P}$, $k_{s,plate}$: R_G , $a_{H,W}$)

Call InnerBulkWall ($a_{H,W}$, $k_{s,sphere}$, d_p , $\omega_{0,wall}$: $R_{B,in1,2,W}$)

Call MidBulkWall ($a_{H,W}$, $r_{eq,wall}$, $k_{s,sphere}$, d_p , $\omega_{0,wall}$, $radius_{\lambda,wall}$: $R_{B,mid1,2,W}$)

Call LambdaGasWall (k_f , $\omega_{0,wall}$, j_{gas} , r_p , $radius_{\lambda,wall}$, $a_{H,W}$: $R_{lambda,W}$)

Call BulkGasWall (r_p , $\omega_{0,wall}$, $radius_{\lambda,wall}$, k_f : $R_{G,W}$)

Call OuterBulkWall (r_p , $\omega_{0,wall}$, $radius_{\lambda,wall}$, $\lambda_{meanfree}$, $k_{s,sphere}$: $R_{G,W}$, $a_{H,W}$, $B_{out,W}$)

$$R_{T,W} = \left[\frac{1}{R_{B,in1,2,W}} + \frac{1}{R_{B,mid1,2,W}} + \frac{1}{R_{B,out1,2,W}}\right]^{-1}$$

$$R_{m,comb,W} = \left[\frac{1}{R_{L,W}} + \frac{1}{R_{\lambda W}} + \frac{1}{R_{G,W}}\right]^{-1}$$

$$R_{j,W} = R_{T,W} + R_{m,comb,W}$$

Call RadiationShortBulk (N_c , d_p , σ_r , T_K , $\varepsilon_{r,1}$, $F_{12,bulk}$, f_k , $\phi_{b,rad}$: $k_{e,r,S}$)

Call RadiationLongBulk (d_p , σ_r , T_K , $\varepsilon_{r,1}$, $F_{12,bulk,eff}$, f_k : $k_{e,r,L}$)

Call RadiationShortWall (d_p , σ_r , T_K , $\varepsilon_{r,1}$, $\varepsilon_{r,2}$, f_k , SW_{WS} , $F_{12,wall,Short}$, $F_{21,wall,Short}$: $k_{e,r,S,W}$)

Call RadiationLongWall (d_p , σ_r , T_K , $\varepsilon_{r,1}$, $\varepsilon_{r,2}$, $F_{12,wall,eff}$, f_k : $k_{e,r,L,W}$)

$$A_c = d_p^{\,2}$$

$$k_{e,c} = \frac{N_c}{2} \cdot \left[\frac{d_p - \omega_{0,bulk}}{R_j \cdot A_c}\right] \cdot \sin(\phi_{b,rad})$$

$$k_{e,r} = k_{e,r,S} + k_{e,r,L}$$

$$k_{eff,bulk} = k_{e,c} + k_{e,r}$$

$$k_{e,r,W} = \mathbf{If}(SW_{WS}\ ,\ 1\ ,\ k_{e,r,S,W},\ k_{e,r,S,W} + k_{e,r,L,W},\ k_{e,r,S,W} + k_{e,r,L,W})$$

$$k_{e,c,W} = \frac{r_p - \omega_{0,wall}}{d_p^{\,2} \cdot R_{j,W}}$$

$$k_{eff,wall} = k_{e,r,W} + k_{e,c,W}$$

$$\frac{k_{eff,ZS}}{k_f} = 1 - \left[\sqrt{1-\varepsilon}\right] + \left[\frac{2 \cdot \left(\sqrt{1-\varepsilon}\right)}{1 - \kappa^{-1} \cdot B}\right] \cdot \left[\left(\frac{(1 - \kappa^{-1}) \cdot B}{(1 - \kappa^{-1} \cdot B)^2}\right) \cdot \ln\left(\frac{1}{\kappa^{-1} \cdot B}\right) - \left(\frac{B+1}{2}\right) - \left(\frac{B-1}{1 - \kappa^{-1} \cdot B}\right)\right]$$

$$B = 1.25 \cdot \left[\frac{1-\varepsilon}{\varepsilon}\right]^{\left[\frac{10}{9}\right]}$$

$$k_{e,ZS,cond} = k_{eff,ZS} + k_{eff,contact}$$

$$\kappa = \frac{k_{s,sphere}}{k_f}$$

$$\frac{k_{eff,contact}}{k_{s,sphere}} = \left[3 \cdot \left(\frac{1 - \mu_{sphere}^{\,2}}{4 \cdot E_{young,sphere}}\right) \cdot f \cdot r_p\right]^{(1/3)} \cdot \frac{1}{0.531 \cdot S} \cdot \frac{N_{A1}}{N_{L1}}$$

Call Contact$_{Kavainy}$ (ε , d_p : $k_{e,r,L,W}$, $a_{H,W}$, $B_{out,W}$, N_{L1})

$$f = F_{bah}$$

$$k_{r,ZS} = \left[\left(1 - (1-\varepsilon)^{0.5}\right) \cdot \varepsilon + \left(\left[\frac{(1-\varepsilon)^{0.5}}{\frac{2}{\varepsilon_{r,1}} - 1}\right] \cdot \left[\frac{B+1}{B}\right]\right) \cdot \left(\frac{1}{1 + \frac{1}{\left[\frac{2}{\varepsilon_{r,1}} - 1\right] \cdot \Lambda}}\right)\right] \cdot 4 \cdot \sigma_r \cdot T_K^{\,3} \cdot d_p$$

$$\Lambda = \frac{k_{s,sphere}}{4 \cdot \sigma_r \cdot T_K^{\,3} \cdot d_p}$$

$$k_{eff,ZS,tot} = k_{e,ZS,cond} + k_{r,ZS}$$

$$B_R = 0.0949306 - 0.14456 \cdot \varepsilon_{r,1} + 0.106337 \cdot \varepsilon_{r,1}^{\,2} + 0.0159144 \cdot \varepsilon_{r,1}^{\,3} - 0.0325521 \cdot \varepsilon_{r,1}^{\,4}$$

$$B_{R,0} = 0.09$$

$$F_E = \frac{2 \cdot B_R + \varepsilon_{r,1} \cdot (1 - B_R)}{(1 - B_R) \cdot (2 - \varepsilon_{r,1})}$$

$$F_{E,0} = \frac{\varepsilon_{r,1}}{2 - \varepsilon_{r,1}}$$

$$\Delta_0 = \frac{F_E \cdot (1 - B_{R,0}) - B_{R,0}}{F_{E,0} \cdot (1 - B_{R,0})}$$

$$d_\theta = \left[\frac{0.523}{1-\varepsilon}\right] \cdot d_p$$

$$d_{\theta,f} = \frac{d_\theta}{1 + \pi}$$

$$d_{\theta,s} = \frac{\pi \cdot d_\theta}{1 + \pi}$$

$$\chi = \frac{F_{E,0}}{F_E}$$

$$k_{eff,RO} = 4 \cdot F_E \cdot \sigma_r \cdot d_\theta \cdot T_K^{\,3} \cdot \left[1 - \chi \cdot \left(\frac{\Delta_0}{1 + \frac{\frac{k_{s,sphere}}{d_{\theta,s}}}{4 \cdot F_{E,0} \cdot \sigma_r \cdot T_K^{\,3} + \frac{k_f}{d_{\theta,f}}}} \right) \right] + k_f \cdot \frac{d_\theta}{d_{\theta,f}} \cdot \left[1 - \left(\frac{\Delta_0}{1 + \frac{\frac{k_{s,sphere}}{d_{\theta,s}}}{4 \cdot F_E \cdot \sigma_r \cdot T_K^{\,3} + \frac{k_f}{d_{\theta,f}}}} \right) \right]$$

$$s_{RO} = 0.0085$$

$$k_{eff,RO,s} = (1 - s_{RO}) \cdot k_{eff,RO} + s_{RO} \cdot k_{s,sphere}$$

$$k_{e,RO} = \frac{k_{eff,RO,s}}{k_f}$$

$$F_{RO} = F_E \cdot \left[1 - \chi \cdot \left(\frac{\Delta_0}{1 + \frac{k_{s,sphere}}{4 \cdot F_{E,0} \cdot \sigma_r \cdot T_K^{\,3} \cdot d_{\theta,s}}} \right) \right]$$

$$k_{RO} = F_{RO} \cdot 4 \cdot d_\theta \cdot \sigma_r \cdot T_K^{\,3}$$

REFERENCES

ABOU-SENA, A., YING, A., ABDOU, M., 2007, Experimental Measurements of the Effective Thermal Conductivity of a Lithium Titanate (Li_2TiO_3) Pebbles-packed Bed, Journal of Materials Processing Technology, Vol. 181, pp. 206–212.

ADAMS, D.J., MATHESON, A.J., 1972, Computation of Dense Random Packings of Hard Spheres, Journal of Chemical Physics, Vol. 56, pp. 1989–1994.

AICHLMAYR, H.T., KULACKI, F.A., 2006, Effective Conductivity of Saturated Porous Media. In **GREEN, G.A.,** Advances in Heat Transfer, Vol. 39, pp. 377–460.

AICHLMAYR, H.T., 1999, The Effective Thermal Conductivity of Saturated Porous Media. University of Minnesota, Master thesis.

ANTONETTI, V.W., WHITE, T.D., SIMONS, R.E., 1991, An approximate thermal contact conductance correlation, ASME 28th National Heat Transfer Conference, Minneapolis, Minnesota, HTD-Vol. 170, pp. 35—42.

ARGENTO, C., BOUVARD, D., 1996, A Ray Tracing Method for Evaluating the Radiative Heat Transfer in Porous Media, International Journal of Heat and Mass Transfer, Vol. 39, pp. 3175–3180.

ARGO, W.B., SMITH, J., 1957, Heat Transfer in Packed Beds, Chemical Engineering Progress, Vol. 49, pp. 443–451.

BAHRAMI, M., 2004, Modeling of Thermal Joint Resistance for Sphere-Flat Contacts in a Vacuum, PhD Dissertation, University of Waterloo, pp. 1-226.

BAHRAMI, M., CULHAM, J.R., YOVANOVICH, M.M., SCHNEIDER, G.E., 2006, Review of Thermal Joint Resistance Models for Nonconforming Rough Surfaces, Applied Mechanics Reviews, Vol. 59, pp. 1–12.

BAHRAMI, M., YOVANOVICH, M.M., CULHAM, J.R., 2004a, Thermal Joint Resistance of Conforming Rough Surfaces with Gas-filled Gaps, Journal of Thermophysics and Heat Transfer, Vol. 18, pp. 318–325.

BAHRAMI, M., YOVANOVICH, M.M., CULHAM, J.R., 2004b, Thermal Joint Resistance of Nonconforming Rough Surfaces with Gas-filled Gaps, Journal of Thermophysics and Heat Transfer, Vol. 18, pp. 326–332.

BAHRAMI, M., YOVANOVICH, M.M., CULHAM, J.R., 2006, Effective Thermal Conductivity of Rough Spherical Packed Beds, International Journal of Heat and Mass Transfer, Vol. 49, pp. 3691–3701.

BARTHELS, H., SCHÜRENKRÄMER, M., 1984, Die effective Wärmeleitfähigkeit in Kugelschüttungen unter besonderer Berücksichtigung des Hochtemperatu-reaktors, Jül-1893, Nuclear Research Centre Jülich.

BATCHELOR, G.K., O'BRIEN, R.W., 1977, Thermal or Electrical Conduction through A Granular Material. Proc. R. Soc. London, Ser. A, Vol. 355, pp. 313–333.

BAUER, R., SCHLÜNDER, E.U., 1978, Effective Radial Thermal Conductivity of Packings in

Gas Flow. Part II. Thermal Conductivity of the Packing Fraction without Gas Flow, International Chemical Engineering, Vol. 18, pp.189-204

BAUER, R., 1990, Stagnant packed beds. *Hemisphere Handbook of Heat Exchanger Design,* **HEWITT, G.F.,** Hemisphere Publishing Corporation, Washington, pp. 2.8.1-1–2.8.4-14.

BENENATI, R.F., BROSILOW, C.R., 1962, Void Fraction Distribution in Beds of Spheres, AIChE Journal, Vol. 8, pp. 359–361.

BERNAL, J.D., MASON, J., 1960, Co-ordination of Randomly Packed Spheres, Nature, London, Vol. 188, pp. 910.

BEVINGTON, P.R., ROBINSON, D.K., 2003, Data Reduction and Error Analysis. Third Edition, McGraw Hill.

BREITBACH, G., BARTHELS, H., 1980, The Radiant Heat Transfer in the High Temperature Reactor Core After Failure of the Afterheat Removal Systems, Nuclear Technology, Vol. 49, pp. 392–399.

BREITBACH, G., 1978, Wärmetransportvorgänge unter besonderer Berücksichtigung der Strahlung, Jül-1564, Nuclear Research Centre Jülich.

BUONANNO, G., CAROTENUTO, A., GIOVINCO, G., MASSAROTTI, N., 2003, Experimental and Theoretical Modeling of the Effective Thermal Conductivity of Rough Steel Spheroid Packed Beds, Journal of Heat Transfer, Vol. 125, pp. 693-702.

COHEN, Y., METZNER, A.B., 1981, Wall Effects in Laminar Flow of Fluids through Packed Beds, AIChE Journal, Vol. 8, pp. 359–361.

CHEN, C.K., TIEN, C.L., 1973, Conductance of Packed Spheres in Vacuum, ASME Journal of Heat Transfer, Vol. 95, pp. 302–308.

CHEN, J.C., CHURCHILL, S.W., 1963, Radiant Heat Transfer in Packed Beds, AIChE Journal, Vol. 9, pp. 35–41.

CHENG, G.J., YU, A.B., ZULLI, P., 1999, Evaluation of Effective Thermal Conductivity from the Structure of a Packed Bed, Chemical Engineering Science, Vol. 54, pp. 4199–4209.

CHENG, G.J., YU, A.B., ZULLI, P., XU, D.L., 2002, Radiation Heat Transfer in Random Packing of Mono-sized Spheres, Proceedings of the 4th World Congress on Particle Technology, Paper No. 313, Sydney, Australia.

CHENG, P., HSU, C.T., 1986, Fully-developed, Forced Convection Flow through an Annular Packed-sphere Bed with Wall Effects, International Journal of Heat and Mass Transfer, Vol. 29, pp. 1843–1853.

DIECK, R.H., 2007, Measurement Uncertianty, ISA, Fourth Edition.

DEISSLER, R.G., BOEGLI, J.S., 1958, An Investigation of Effective Thermal Conductivities of Powders in Various Gases, ASME Transactions, Vol. 80, No. 7, pp. 1417–1425.

DE KLERK, A., 2003, Voidage Variation in Packed Beds at Small Column to Particle Diameter Ratio, AIChE Journal, Vol. 49, pp. 2022–2029.

DU TOIT, C.G., 2002, The Numerical Determination of the Variation in the Porosity of the Pebble-bed Core, Proceedings of HTR2002, pp. 1–5.

DU TOIT, C.G., 2008, Radial Variation in Porosity in Annular Packed Beds, Nuclear Engineering and Design, pp. 3073–3079.

DU TOIT, C.G., VAN ANTWERPEN, W., ROUSSEAU, P.G., 2009, Analysis of the Porous Structure of an Annular Pebble Bed Reactor, Proceedings of ICAPP09 – ID9123, pp. 1-10.

GOTOH, K., 1978, J. Soc. Pow. Tech., Japan, Vol. 15, pp. 220.

GOODLING, J.S., VACHON, R.I., STELPFLUG, W.S., YING, S.J., 1983, Radial Porosity Distribution in Cylindrical Beds Packed with Spheres, Powder Technology, Vol. 35, pp. 23–29.

GOODLING, J.S., KHADER, M.S., 1985, Co-ordination Number Distribution of Spherical Particles in a Packed Cylindrical Bed, Powder Technology, Vol. 44, pp. 53–55.

HAUGHEY, D.P., BEVERIDGE, G.S.G., 1969, Structural Properties of Packed Beds: A Review, Canadian Journal of Chemical Engineering, Vol. 47, pp. 130–140.

HINRICHSEN, H., WOLF, D.E., 2006, The Physics of Granular Media, Wiley, Weinheim.

HOLTON, W.C., 2005, Environmental Health Perspectives, Web article, http://findarticles.com/p/articles/mi_m0CYP/is_11_113/ai_n15956767/

HSU, C.T., CHENG, P., WONG, K.W., 1995, A Lumped-parameter Model for Stagnant Thermal Conductivity of Spatially Periodic Porous Media, ASME Journal of Heat Transfer, Vol. 117, pp. 264–269.

HSU, C.T., CHENG, P., WONG,K.W., 1994, Modified Zehner-Schlunder Models for Stagnant Thermal Conductivity of Porous Media, International Journal of Heat and Mass Transfer, Vol.37, pp. 2751-2759.

HUNT, M.L., TIEN, C.L., 1990, Non-Darcian Flow, Heat and Mass Transfer in Catalytic Packed-bed Reactors, Chemical Engineering Science, Vol. 45, pp. 55–63.

HOWELL, J.R., 2000, Radiative Transfer in Porous Media, Chapter 15, **VAFAI, K.,** Handbook of Porous Media, First Edition, ISBN 0-8247-8886-9

INCROPERA, F.P., DE WITT, D.P., 2002, Fundamentals of Heat and Mass Transfer, 5th Edition, Wiley, Hoboken NJ.

JONES, L.R., 1965, Diffuse Radiation View Factors between Two Spheres, ASME Journal of Heat Transfer, Vol. 87, pp. 421–422.

KAMIUTO, K., NAGUMO, Y., IWAMOTO, M., 1989, Mean Effective Thermal Conductivities of Packed-sphere Systems, Applied Energy, Vol. 34, pp. 213.

KASPAREK, G., 1975, Wärmestrahlung in Kugelschüttungen: Experiment und Theorie, Dissertation Technical University of München.

KASPAREK, G., VORTMEYER, D., 1976, Wärmestrahlung in Schüttungen aus Kugeln mit Vernachlässigbarem Wärmeleitwiderstand, Wärme- und Stoffübertrgung, Vol. 9, pp. 117–128.

KAVIANY, M., 1991, Principles of Heat Transfer in Porous Media, Springer, New York.

KENNARD, E.H., 1938, Kinetic Theory of Gases, McGraw-Hill, New York.

KITSCHA, W.W., YOVANOVICH, M.M., 1974, Experimental Investigation on the Overall

Thermal Resistance of Sphere-Flat Contacts, AIAA 12th Aerospace Science Meeting, Washington, D.C., pp.93-110.

KTA (NUCLEAR SAFETY STANDARDS COMMISSION), 1981, KTA 3102.3 Reactor Core Design of High-temperature Gas-cooled Reactors, Part 3: Loss of Pressure through Friction in Pebble Bed Cores, Germany.

KUGELER, K., SCHULTEN, R., 1989, Hochtemperaturreaktortechnik, Springer-Verlag, Heidelberg.

KUNII, D., SMITH, J.M., 1960, Heat Transfer Characteristics of Porous Rocks, AIChE Journal, Vol. 6, No. 1, pp. 71–78.

LAMBERT, M.A., FLETCHER, L.S., 1997, Thermal contact conductance of spherical rough metals, Journal of Heat Transfer, ASME, vol. 119, no. 4, pp. 684–690.

LOCHMANN, K., OGER, L., STOYAN, D., 2006, Statistical Analysis of Random Sphere Packings with Variable Radius Distribution, Solid State Sciences, Vol. 8, pp. 1397–1413.

LEE, S.H.-K., IP, S.C.-H., WU, A.K.C., 2001, Sphere-to-Sphere Radiative Transfer Coefficient for Packed Sphere System, ASME International Mechanical Engineering Congress and Exposition, pp. 105–110.

LIU, F.L., ZHANG, Z.P., YU, A.B., 1999, Dynamic Simulation of the Centripetal Packing of Mono-sized Spheres, Physica A, Vol. 268, pp. 433–453.

LU, Z., 2000, Numerical Modelling and Experimental Measurement of the Thermal and Mechanical Properties of Packed Beds. University of California, Ph.D. thesis.

MARTIN, H., 1978, Low Peclet Number Particle-to-Fluid Heat and Mass Transfer in Packed Beds, Chemical Engineering Science, Vol. 33, pp. 913–919.

MEISSNER, H.P., MICHEALS, A.S., KAISER, R., 1964, Crushing Strength of Zinc Oxide Agglomerates, I&EC Process Design and Development, Vol. 3, pp. 202–205.

MODEST, M.F., 1993, Radiative Heat Transfer, McGraw-Hill.

MUELLER, G.E., 1992, Radial Void Fraction Distribution in Randomly Packed Fixed Beds of Uniformly Sized Spheres in Cylindrical Containers, Powder Technology, Vol. 72, pp. 269–275.

MUELLER, G.E., 1999, Radial Void Fraction Correlation for Annular Packed Beds, AIChE Journal, Vol. 45, pp. 2458–246.

NAKAGAKI, M., SUNADA, H., 1968, Theoretical Studies on Structures of the Sedimentation Bed of Spherical Particles, Yakugaku Zasshi, Vol. 88, pp. 651–655.

NAYAK, A.L., TIEN, C.L., 1978, A Statistical Thermodynamic Theory for Coordination-number Distribution and Effective Thermal Conductivity of Randomly Packed Beds, International Journal of Heat and Mass Transfer, Vol. 21, pp. 669–676.

NIELD, D.A., 1991, Estimation of the Stagnant Thermal Conductivity of Saturated Porous Media, International Journal of Heat and Mass Transfer, Vol. 34, pp. 1575–1576.

NIESSEN, H.F., BALL, S., 2000, IAEA-TECDOC-1163: Heat Transport and Afterheat Removal for Gas Cooled Reactors Under Accident Conditions.

http://www.iaea.org/inisnkm/nkm/aws/htgr/fulltext/crp3.pdf

NOZAD, S., CARBONELL, R.G., WHITETAKER, S., 1985, Heat Conduction in Multiphase Systems, I: Theory and Experiments for Two-phase Systems, Chemical Engineering Science, Vol. 40, pp. 843–855.

NOZAD, S., CARBONELL, R.G., WHITETAKER, S., 1985, Heat Conduction in Multiphase Systems, II: Experimental Method and Results for Three-phase Systems, Chemical Engineering Science, Vol. 40, pp. 857–863.

OKAZAKI, M, YAMASAKI, T., GOTOH, S., TOEI, R., 1981, Effective Thermal Conductivity for Granular Beds of Various Binary Mixtures, Journal of Chemical Engineering of Japan, Vol. 14, pp. 183–189.

OKAZAKI, M., ITO, I., TOEI, R, 1977, Effective Thermal Conductivities of Wet Granular Materials, AIChE Symposium Series 73, Vol. 163, pp. 164–176.

OXFORD INTERNATIONAL BIOMEDICAL CENTRE (OIBC) REPORT, 2008, Alternative Energy, Health and the Environment, pp.1-12.

PEBBLE BED MODULAR REACTOR (Pty) Limited (PBMR), 2009, web:http://www.pbmr.co.za/.

PITSO, M.L., 2009, Private Communication.

POLSON, A., 2006, Private Communication.

PRASAD, V., KLADIAS, N., BANDYOPADHAYA, A., TIAN, Q., 1989, Evaluation of Correlations for Stagnant Thermal Conductivity of Liquid-saturated Porous Beds of Spheres, International Journal of Heat and Mass Transfer, Vol. 32, pp. 1793–1796.

RIDGEWAY, K., TARBUCK, K.J., 1968, Voidage Fluctuations in Randomly-packed Beds of Spheres Adjacent to a Containing Wall, Chemical Engineering Science, Vol. 23, pp. 1147–1155.

ROBOLD, K., 1982, Wärmetransport im Inneren und in der Randzone von Kugelschüttungen, Dissertation Jül-1796, Nuclear Research Centre Jülich.

ROUSSEAU, P.G., VAN STADEN, M., 2008, Introduction to the PBMR heat transfer test facility, Nuclear Engineering and Design, Vol.238, pp. 3060-3072.

RUMPF, J., 1958, Chem.-Ing.-Techn., Vol. 30, pp. 144.

SHAPIRO, M., DUDKO, V., ROYSEN, V., KRICHEVETS, Y., LEKHTMAKHER, S., GROZUBINSKY, V., SHAPIRA, M., BRILL, M., 2004, Characterization of Powder Beds by Thermal Conductivity: Effect of Gas Pressure on the Thermal Resistance of Particle Contact Points, Part. Part. Syst. Charact., Vol. 21, pp. 268–275.

SHONNARD, D.R., WHITETAKER, S., 1989, The Effective Thermal Conductivity for a Point-contact Porous Medium: An Experimental Study, International Journal Of Heat and Mass Transfer, Vol. 32, pp. 503–512.

SINGH, B.P., KAVIANY, M., 1994, Effect of Solid Conductivity on Radiative Heat Transfer in Packed Beds, International Journal of Heat and Mass Transfer, Vol. 37, pp. 2579–2583.

SIU, W.W.M., LEE, S.H.-K, 2000, Effective Conductivity Computation of a Packed Bed Using Constriction Resistance and Contact Angle Effects, International Journal of Heat

and Mass Transfer, Vol. 43, pp. 3917–3924.

SLAVIN, A.J., ARCAS, V., GREENHALGH, C.A., IRVINE, E.R., MARSHALL, D.B., 2002, Theoretical Model for the Thermal Conductivity of a Packed Bed of Solid Spheroids in the Presence of a Static Gas, with no Adjustable Parameters Except at Low Pressure and Temperature, International Journal of Heat and Mass Transfer, Vol. 45, pp. 4151–4161.

SMITH, W.O., FOOTE, P.D., BUSANG, P.F., 1929, Packing of Homogeneous Spheres, Physical Review, Vol. 34, pp. 1271–1274.

SMOLUCHOWSKI, M., 1898, Annalen der Physik, Vol. 64, pp. 101.

SODRÉ, J.R., PARISE, J.A.R., 1998, Fluid Flow Pressure Drop through an Annular Bed of Spheres with Wall Effects, Experimental Thermal and Fluid Science, Vol. 17, pp. 265–275.

SPRINGER, G.S., 1971, Heat Transfer in Rarefied Gases, Advances in Heat Transfer, Vol. 7, pp. 163–218.

STÖCKER, B., 1998, Untersuchungen zur selbsttätigen Nachwärmeabfuhr bei Hochtemperaturreaktoren unter besonderer Berücksichtigung der Naturkonvektion, Jül-3504, Nuclear Research Centre Jülich.

STRIEDER, W., 1997, Radiation Heat Transport in Disordered Media, Advances in Water Resources, Vol. 20, pp. 171–187.

SUZUKI, M., MAKINO, K., YAMADA, M., IINOYA,K., 1981, A Study on the Coordination Number in a System of Randomly Packed, Uniform-sized Spherical Particles, International Chemical Engineering, Vol. 21, pp. 482–488.

TANEMURA, M., 1986, On the Stereology of the Radial Distribution Function of Hard-sphere Systems, Proceedings of the First International Symposium for Science on Form, pp. 157–165.

TANNER, L.H., FAHOUM, M., 1976, A study of the surface parameters of ground and lapped metal surfaces, using specular and diffuse reflection of laser light, Wear, Vol.36, pp. 299-316.

THURGOOD, C.P., AMPHLETT, R.F., MANN, R.F., PEPPLEY, B.A., 2003, Radiative Heat Transfer in Packed-beds: The Near-wall Region. Proceedings of AIChE Spring National Meeting, pp. 257–269.

THEUERKAUF, J., WITT, P., SCHWESIG, D., 2006, Analysis of Particle Porosity Distribution in Fixed Beds Using the Discrete Element Method, Powder Technology, Vol. 165, pp. 92–99.

TORQUATO, S., 1987, Thermal Conductivity of Disordered Heterogeneous Media from the Microstructure, Reviews in Chemical Engineering, Vol. 4, pp. 151–204.

TSOTSAS, E., MARTIN,H., 1987, Thermal Conductivity of Packed Beds: A Review, Chem. Engineering Processes, Vol. 22, pp. 19–37.

TSOTSAS, E., 2002, *Hemisphere Handbook of Heat Exchanger Design,* **HEWITT, G.F.,** Hemisphere Publishing Corporation, Washington, pp. 2.8.2.

VAN ANTWERPEN, H.J., 2009, Derivation of a dimensionless correlation for effective

thermal conductivity from the HTTU. M-Tech Industrial document, HTTU002-0055, pp. 1-34.

VAN ANTWERPEN, H.J., 2007, Modelling a pebble bed High Temperatrure Gas-coolded Reactor using a system-CFD approach. PhD thesis.

VAN ANTWERPEN, W., ROUSSEAU, P.G., DU TOIT, C.G., 2009, Accounting for Porous Structure in Effective Thermal Conductivity in a Pebble Bed Reactor. Proceedings of ICAPP09 – ID9124, pp. 1-12.

VAN ANTWERPEN, W., 2009 (a), Modeling Effective Thermal Conductivity in Packed Bed Reactors for the Bulk and Near-wall Regions. IYCE2009 Conference Proceedings, pp. 1-8.

VAN ANTWERPEN, W., 2009 (b), High Temperature Test Unit (HTTU) Test Report for Nitrogen Near Vacuum High Temperature (1200 °C) Tests. M-Tech Industrial document, HTTU002-0045, pp. 1-34.

VAN ANTWERPEN, W., DU TOIT, C.G., ROUSSEAU, P.G., 2010, A Review of Correlations to Model the Packing Structure and Effective Thermal Conductivity in Packed Beds of Mono-sized Spherical Particles. Nuclear Engineering and Design, Vol. 240, pp. 1083-1818.

VAN DER MERWE, J., VAN ANTWERPEN, H.J., MULDER, E.J., 2006, Heat Transfer Correlation Limitations at the Pebble Bed Reflector Interface, Proceedings of HTR2006, C00000130.

VON DER DECKEN, C.B., LANGE, G., 1990, AVR – Experimental High Temperature Reactor: 21 Years of Succesfull Operation, Chapter 3.3, pp. 154-169.

VORTMEYER, D., 1966, Wärmestrahlung in Kugelschüttungen, VDI-Fortschrittsberichte, Chemie-Ing. –Techn., Vol. 38, pp. 404–406.

VORTMEYER, D., 1978, Radiation in Packed Solids, Proceedings of 6th International Heat Transfer Conference (Toronto), Vol. 6, pp. 525–539.

VORTMEYER, D., BOERNER, C.J., 1966, Die Strahlungsdurchlasszahl in Schüttungen, VDI-fortschrittsberichte, Chemie-Ing. –Techn., Vol. 38, pp. 1077–1079.

VORTMEYER, D., SCHUSTER, J., 1983, Evaluation of steady flow profiles in rectangular and circular packed beds by a variational method, Chemical Engineering Science, Vol. 38, pp. 1691–1699.

WAKAO, N., KATO, K., 1968, Effective Thermal Conductivity of Packed Beds, Journal of Chemical Engineering of Japan, Vol. 2, pp. 24–33.

WHITE, S.M., TIEN, C.L., 1987, Analysis of Flow Channeling Near the Wall in Packed Beds, Wärme- und Stoffübertragung, Vol. 21, pp. 291–296.

YAGI, S., KUNII, D., 1957, Studies on Effective Thermal Conductivities in Packed Beds, AIChE Journal, Vol. 3, pp. 373–377.

YAGI, S., KUNII, D., 1961, Fluidized-solids Reactors with Continuous Solids Feed—I: Residence Time of Particles in Fluidized Beds, Chemical Engineering Science, Vol. 16, pp. 364–371.

YANG, R.Y., ZOU, R.P., YU, A.B., 2000, Computer Simulation of the Packing of Fine Particles, Physical Review E, Vol. 62, pp. 3900–3908.

YOVANOVICH, M.M., 1982, Thermal Contact Correlations, *Spacecraft Radiative Transfer and Temperature Control*, edited by T. E. Horton, Progress in Aeronautics and Aerodynamics, Vol. 83, AIAA, New York, pp. 83–95.

YOVANOVICH, M.M., MAROTTA, E.E., 2006, Thermal Spreading and Contact Resistances, *Heat Transfer Handbook*, **BEJAN, A., KRAUS, A.D.,** Wiley, Hoboken, NJ, pp. 261–393.

ZEHNER, P., SCHLÜNDER, E.U., 1970, Wärmeleitfähigkeit von Schüttugen bei mäßigen Temperaturen, Chemie-Ing. –Techn., Vol. 42, pp. 933–941.

ZEHNER, P., SCHLÜNDER, E.U., 1972, Einfluß der Wärmestrahlung und des Druckes auf den Wärmetransport in nicht durchströmten Schüttugen, Chemie-Ing. –Techn., Vol. 44, pp. 1303–1308.

ZHANG, Z.P., LIU, L.F., YUAN, A.B., YU, A.B., 2001, A Simulation Study of the Effects of Dynamic Variables on the Packing of Spheres, Powder Technology, Vol. 116, pp. 23–32.

ZHOU, J., YU, A.B., ZHANG, Y., 2007, A Boundary Element Method for Evaluation of the Effective Thermal Conductivity of Packed Beds, Journal of Heat Transfer, Vol. 129, pp. 363–371.

ZOU, R.P., YU, A.B., 1995, The Packing of Spheres in a Cylindrical Container: The Thickness Effect, Chemical Engineering Science, Vol. 50, pp. 1504–1507.